Title: Living with high potassium: how plants balance nutrient acquisition during K-induced salt stress

Pramod Pantha[1], Dong-Ha Oh[1], David Longstreth[1] and Maheshi Dassanayake[1,*]

[1]Department of Biological Sciences, Louisiana State University, Baton Rouge, LA 70803, USA

*Address correspondence to: maheshid@lsu.edu

Short title: Avoiding N starvation upon high K stress

Abstract

K is more toxic in plants than Na at similar concentrations but the molecular mechanisms governing excess K-induced salt stress are unknown. We used *Arabidopsis thaliana* and its extremophyte relative *Schrenkiella parvula*, to explore this largely unexplored question using comparative physiological, ionomic, transcriptomic, and metabolomic approaches aimed at understanding how plants can develop resilience to excess K. Our results showed that the stress responses exhibited by the two plants diverged at a decisive step where the stress-sensitive *A. thaliana* could not limit excess K influx and suffered severe nutrient depletion. The stress adapted model, *S. parvula*, was able to independently regulate reduction in K uptake while sustaining uptake of other major nutrients including N. Maintaining N uptake and its uninterrupted assimilation into primary metabolites allowed *S. parvula* to sustain growth and concurrently boost its antioxidant and osmolyte pools, facilitated by a targeted transcriptomic response. In contrast, *A. thaliana* descended into mismanaged transcriptional cascades including induction of biotic and abiotic stress responses and autophagy accompanied by inhibited growth, reduced photosynthesis, and increased ROS. This study provides a basic framework to select key pathways to target in the development of building plant resilience towards nutrient imbalance caused by K-induced salt stress.

Keywords

K-induced salt stress, potassium transport, transcriptomics, metabolomics, ionomics, molecular phenotype, abiotic stress, nitrogen metabolism, osmoprotectants, antioxidants, antagonistic pleiotropy

Introduction

Can excess potassium (K) in soil be too much of a good thing for plants? Its role as an essential macronutrient for plants is well established and K constitutes 2-10% of plant dry weight (Wang and Wu, 2013). The cytosolic concentration of K^+ is around 100 mM and the vacuolar concentrations generally range between 20-200 mM depending on tissue, developmental age, or species (Leigh and Wyn Jones, 1984; Ashley et al., 2006). These concentrations are typically higher than soil concentrations found in most agricultural soils (Maathuis, 2009) and therefore the vast majority of studies have only investigated uptake into plants from low K^+ concentrations in the soil. As a result, we hardly know if excess K^+ in soils would be as toxic as high Na^+ (Pantha and Dassanayake, 2020), and if it is, how it exerts plant toxicity effects that may be different from Na-induced salt stress seen for high salt concentrations known to cause plant toxicity (>100 mM NaCl). While toxicity in plants growing at high concentration of other nutrients, such as boron (Aquea et al., 2012; Wang et al., 2021), copper (Lequeux et al., 2010), and nitrogen (Yoshitake et al., 2021), have been investigated, the molecular mechanisms behind high K^+ responses are virtually unknown.

The need to use alternative agricultural lands and recycled wastewater amidst diminishing freshwater resources is intense (IPCC, 2019). These needs cannot be addressed without foundational knowledge of how plant nutrient balance is achieved when conventional land use and irrigation practices no longer provide adequate solutions. Worldwide there are many regions that are naturally high in soil K^+ content (Duval et al., 2005; Warren, 2016). Many industrial as well as agricultural processing plants produce wastewater with exceptionally high K^+ concentrations considered excessive for plant growth (Arienzo et al., 2009). During wastewater treatments, unlike N, P, or organic matter which are typically processed using microbial activity, K is concentrated due to evaporation (Arienzo et al., 2009). Therefore,

59 knowing the tolerance mechanisms against high K, which can cause osmotic stress similar to Na
60 on top of additional stresses because of its role as a major nutrient in plants, are imperative
61 toward designing robust crops in our quest to convert marginal lands into productive
62 agricultural lands and reclaim land left unusable due to irrigation practices such as the use of
63 recycled wastewater.

64 How high K^+ in soils affect plant growth is not a new question for plant scientists (Eijk,
65 1939). Past studies have reported that high concentrations of K^+ severely affected growth and
66 other developmental processes when tested in a handful of species. For example, growth of
67 *Salicornia herbacea* was induced by 166, 250, and 333 mM NaCl but reduced when treated with
68 the same concentrations of KCl, implying ion specific detrimental effects of K^+ in a halophyte
69 known to be able to cope with high salinity stress (Eijk, 1939). Additional studies using other
70 halophytes including, *Suaeda aegyptiaca* (Eshel, 1985), *S. salsa* (Wang et al., 2001), and several
71 *Atriplex spp.* (Ashby and Beadle, 1957; Matoh et al., 1986; Ramos et al., 2004) have shown that
72 KCl is more toxic than NaCl at similar osmotic strengths. Recently, Richter et al., (2019)
73 compared the effects of 100 mM NaCl, 50 mM Na_2SO_4, and 100 mM KCl and reported that K^+
74 caused more negative physiological and metabolic responses then Na^+ in *Vicia faba*. These
75 studies suggest that K^+ may not elicit the same physiological, metabolic, or genetic responses
76 Na^+ does and plants may require distinct genetic pathways in addition to canonical salt
77 response pathways (Pantha and Dassanayake, 2020) to survive high K-induced salt stress.

78 In this study, we aimed to identify K-induced salt stress responses and deduce the
79 underlying cellular mechanisms plants have evolved to adapt to K^+ toxicity. We compared
80 *Arabidopsis thaliana* (Col-0 ecotype), a model plant sensitive to high K^+, to its extremophyte
81 relative, *Schrenkiella parvula* (Lake Tuz ecotype) that thrives in high K^+ soils (Nilhan et al., 2008;
82 Oh et al., 2014). We examined multi-omics level features and responses exhibited by the two
83 model species to high K^+ treatments to identify the relevant genetic pathways influential in
84 regulating or are affected by K^+ toxicity responses. Our results revealed an extensive ionomic,
85 metabolic, and transcriptomic reprogramming during high potassium stress in the stress-
86 sensitive model while providing novel insights into how a stress-adapted model had evolved
87 cellular mechanisms to tolerate K^+ toxicity via metabolic and transcriptomic adjustments.

88

89 **Materials and methods**

90 **Plant material, growth conditions, and stress treatments**

91 Plants were grown at 125-150 µmol $m^{-2}s^{-1}$ photon flux density at a photoperiod of 12 h
92 light, 12 h dark, 23°C, and 60% relative humidity for all the experiments unless described
93 otherwise. For transcriptome, ionome, and metabolome profiling, *Arabidopsis thaliana* (Col-0)
94 and *Schrenkiella parvula* (Lake Tuz ecotype) plants were grown hydroponically in 1/5th strength
95 Hoagland's solution as described in Wang et al., 2021. 25-day-old seedlings (days after
96 germination) were transferred to fresh hydroponic growth media at control conditions or
97 supplemented with 150 mM KCl. Samples were harvested at 0, 3, 24, and 72 hours after
98 treatment (HAT) as summarized in Fig S1. Shoot and root tissue samples were harvested on a
99 randomized basis from the same growth chamber, at the same time of day for control and salt-
100 treated plants. Roots were briefly dried with a paper towel to soak any excess growth solution.
101 At least five plants per sample were harvested in at least three biological replicates (Fig S1). All
102 treatment and harvest times were set at 4 h after the beginning of the light cycle to avoid
103 variation due to circadian effects. The salt treatment was non-lethal to both *A. thaliana* and *S.*
104 *parvula* plants based on preliminary tests using a series of salt concentrations.

105 The primary root length, lateral root number and density, and root hair length were
106 quantified using plate-grown seedlings. For this, surface-sterilized seeds were germinated in
107 Petri plates on 1/4th Murashige and Skoog (MS) medium (Murashige and Skoog, 1962) solidified
108 with 0.8% Phyto agar (PlantMedium) and grown for 5 days. The seedlings were transferred to
109 13 cm-diameter large Petri plates with the same media supplemented with different
110 concentration of salts and further incubated in a vertical position to allow better root growth.
111 All measurements were completed before the primary root reached the bottom of the plates.
112 Microscopic images of root hairs were obtained using a Zeiss Lumar brightfield microscope with
113 a 1.5 X FWD 30 mm objective. Plants were imaged for lengths of roots, root hair, and leaf area
114 measurements and quantified using ImageJ (Ferreira and Rasband, 2012). Lateral root density
115 was calculated by dividing the total lateral root number by the total length of the primary root.

116 For the plants grown in soil, seeds were directly germinated in
117 13.75cmx13.75cmx6.87cm pots with SunGro MetroMix 360 soil (SunGro Horticulture, Agawam,
118 MA). The plants were watered with 1/5th strength Hoagland's solution once every week and
119 with tap water every other day. 21 days-old *A. thaliana* and *S. parvula* plants were watered
120 with tap water or 50-400 mM NaCl or KCl salt solutions for control and salt treated plants,
121 respectively, every other day for 14 days.

122 **CO_2 assimilation rates**

123 CO_2 assimilation rates were measured on hydroponically grown plants using a LiCor
124 6400XT portable system attached to a 6400-17 whole plant Arabidopsis chamber mounted with
125 a 6400-18 RGB light source (LiCor Inc, Lincoln Nebraska). Rates were measured on 25-day old *A.*
126 *thaliana* and *S. parvula* plants at 0, 3, 24, and 72 h after exposure to 150 mM KCl. Individual
127 plants were placed in a 15 ml centrifuge tube containing the appropriate treatment solution
128 and the centrifuge tube was inserted into a sealed 38 mm Cone-tainer™ mounted in the whole
129 plant Arabidopsis chamber. The chamber was kept at a slight positive pressure and CO_2
130 exchange was minimal for centrifuge tubes containing nutrient solution with no plants. CO_2
131 assimilation rates were measured at 400 µL L^{-1} CO_2, 1,000 µmol photons m^{-2} s^{-1}, a chamber
132 temperature of 23°C and an air flow rate of 500 mL min^{-1} after CO_2 assimilation rates were
133 constant (usually within 5 minutes for *A. thaliana* and 10 minutes for *S. parvula*).
134 Measurements were made on 3 replicate plants.

135 **Ionome and Total C and N profiling**

136 For each time point and condition described in Fig S1, four biological replicates were
137 harvested and dried for 1 week at 40°C and weighed daily until the dry weights stabilized
138 before grinding. The sample preparation for ionome measurements was performed following
139 Ziegler et al. (2013). Briefly, 10-30 mg of dried samples were digested with 2.5 mL concentrated
140 HNO_3 (AR Select Grade, VWR International, LLC) at room temperature overnight and heated at
141 105°C for 2 h. Each sample was diluted to 10 mL with ultrapure 18MΩ water (UPW) and 0.9 mL
142 of the diluted extract was further mixed with 4.1 mL UPW to a 5 mL final volume, of which 1.2
143 mL was used for ICP-MS (inductively coupled plasma mass spectrometry). Concentrations of 21
144 elements (K, P, Mg, S, Ca, Al, Zn, Co, Ni, Fe, Se, Cu, B, Mn, Mo, As, Rb, Cd, Na, Li, and Sr) were

145 quantified at USDA-ARS-Plant Genetics Facility, Donald Danforth Plant Science Center, as
146 described in Baxter et al. (2014), using a Perkin Elmer NexION ICP-MS platform with 20 µg L^{-1} In
147 as an internal standard (Aristar Plus, BDH Chemicals). Results were visualized as heatmaps using
148 the 'pheatmap' R package (v. 1.0.12) (Kolde, 2012). Total carbon and nitrogen were quantified
149 using a Costech 4010 elemental analyzer (Costech, Valencia, CA, US). Each sample ranged from
150 2-10 mg ground tissue. Acetanilide and 4 mg of wheat flour were used as internal controls.
151 One-way ANOVA, followed by Tukey's post hoc test ($p<0.05$) was performed using the agricolae
152 R package for 3-4 biological replicates to determine elements with significant differences
153 between samples.

154 **Metabolite profiling**

155 To obtain high-throughput metabolite profiles on samples described in Fig S1, we
156 performed non-targeted gas chromatography-mass spectrometry (GC-MS) at the Fiehn
157 Laboratory, West-coast Metabolomics Center at UC-Davis. Following harvest, both root and
158 shoot samples were immediately frozen in liquid nitrogen and processed as described in Fiehn
159 et al. (2008). A Leco Pegasus IV mass spectrometer with the following parameters were used:
160 unit mass resolution at 17 spectra per second with a scan mass range of 85-500 Da at 70 V
161 ionization energy and 1800 V detector voltage with a 230°C transfer line and a 250°C ion
162 source. Raw data files were processed using ChromaTOF software (Version 2.32, Leco) with
163 automatic mass spectral deconvolution followed by peak detection at 5:1 signal/noise levels for
164 all chromatograms. The BinBase database was used for automated annotation of detected
165 peaks to metabolites (https://bitbucket.org/fiehnlab/binbase/src/master/). To generate
166 relative abundance values, we used peak heights of specific retention indices which allows
167 greater separation between metabolites and higher detection capacity for less abundant
168 metabolites. The raw abundance/intensity for each identified compound was normalized with a
169 series of fatty acid methyl esters (xylulose, oleamide, mannonic acid, enolpyruvate,
170 dihydroxymalonic acid, coniferin, butyrolactam, 2-ketoglucose dimethylacetal, and 2,5-
171 dihydroxypyrazine) used as National Institute of Standards and Technology (NIST) internal
172 standards. Significance tests were performed using one-way ANOVA followed by Tukey's post
173 hoc test at $p<0.05$ in the agricolae R package for at least three biological replicates and circular

174 plots to visualize selected metabolites were generated using the circlize package in R (Gu et al.,
175 2014).

176 **RNA-seq analyses**

177 Total RNA from three biological replicates of root and shoot tissues harvested at 0, 3,
178 24, and 72 h after treating with 150 mM KCl (Fig S1) was extracted (~6 µg) using RNeasy Plant
179 Mini Kit (Qiagen, Hilden, Germany) with column digestion to remove DNA contamination. Six to
180 eight plants were pooled for each replicate. A total of 48 RNA-seq libraries were prepared using
181 the TruSeq RNA library preparation kit (Illumina, San Diego, USA) and sequenced on an Illumina
182 HISeq 4000 platform at the Roy J. Carver Biotechnology Center, University of Illinois at Urbana-
183 Champaign. A total of 12-23 million 50-bp reads was obtained from each library (available at
184 NCBI-SRA database under BioProject PRJNA63667). Following quality checks using FastQC
185 (Andrews, 2010), RNA-seq reads uniquely mapped to *A. thaliana* TAIR10 or *S. parvula*
186 (Dassanayake et al., 2011) v2.2 gene models (https://phytozome-next.jgi.doe.gov/), were
187 quantified using Bowtie (Langmead et al., 2009) and a custom script as described in (Pantha et
188 al., 2021).

189 Differentially expressed genes (DEGs) between K^+ treated and control samples were
190 identified using DESeq2 with an adjusted p-value cutoff 0.01 (Love et al., 2014). DEGs shared
191 between treatments were plotted using UpSetR (Conway et al., 2017). Orthologous gene pairs
192 between the two species were identified using the CLfinder-OrthNet pipeline with default
193 settings (Oh and Dassanayake, 2019) and further refined as described in Wang et al. (2021) to
194 include lineage-specific genes and duplications. For ortholog expression comparisons between
195 *S. parvula* and *A. thaliana*, regularized log (rlog) values estimated by DESeq2 were normalized
196 per each gene. Ortholog pairs compared to the median across all samples were used to
197 determine temporal co-expression clusters based on fuzzy k-means clustering (Gasch and Eisen,
198 2002) with a membership cutoff set to 0.5. From initially identified 10 root and 11 shoot
199 clusters (Table S11), we filtered out clusters that did not show a response to K treatments in
200 both species and identified 5 root and 3 shoot co-expression super clusters with distinct
201 response trends. All expressed genes were assigned Gene Ontology (GO) annotations when
202 available and DEGs with GO annotations were used to identify enrichment processes using

203 BinGO (Maere et al., 2005). To summarize functional groups enriched among DEGs, redundant
204 GO terms with > 50% overlap were further clustered using GOMCL (Wang et al., 2020). DEGs
205 were also annotated based on KEGG pathways (Kanehisa et al., 2016). Functional processes
206 identified with specific GO terms which included less than 500 genes to represent a function
207 were used for functional enrichment analysis. Additionally, processes with less than 20 DEGs
208 were removed from downstream analysis. This avoided inclusion of functions represented by
209 fewer genes and any process that had large number of genes that resulted in generic
210 descriptions of the processes. This avoided inclusion of functions represented by a few genes
211 and any process that had large number of genes that resulted in broad or generic descriptions
212 from the comparison. Heatmaps for gene expression visualization were generated using the
213 'pheatmap' R package (v. 1.0.12) (Kolde, 2012).

214 **Histochemical detection of hydrogen peroxide and superoxide**

215 Histochemical detection of H_2O_2 was performed on 25 days-old hydroponically grown *A.*
216 *thaliana* and *S. parvula* plants using 3,3'-diaminobenzidine (DAB, Sigma-Aldrich, Poland) which
217 is oxidized in the presence of H_2O_2 and forms a brown stain (Daudi and O'Brien, 2012). We
218 further assessed the formation of superoxide during high K^+ stress using nitroblue tetrazolium
219 (NBT) (Thermo Fisher Scientific) which in the presence of O_2^- forms a purple stain (Jabs et al.,
220 1996). The DAB and NBT solutions were applied on leaves under a gentle vacuum infiltration for
221 5 minutes followed by shaking at 100 rpm for 4 h. Five mL of 10 mM Na_2HPO_4 without staining
222 solutions was used as a negative control. Staining solutions were replaced with a bleaching
223 solution (ethanol: acetic acid: glycerol = 3:1:1) for destaining chlorophyll by boiling for 15
224 minutes. Destained leaves were imaged using a Zeiss Lumar microscope with x0.8
225 magnification. We tested three plants per condition and two leaves per plant.
226

227 **Results**

228 **KCl is more toxic than NaCl at the same osmotic strengths**

229 Independent of plant age (Fig 1A, S2) and tissue type (Fig 1C-E), K^+ exerts more severe
230 growth disturbances than observed for Na^+ at the same concentrations in both species. For
231 example, *A. thaliana* treated with 100 mM KCl did not survive compared to 100 mM NaCl

232 treated plants while *S. parvula* treated with 400 mM KCl did not flower compared to 400 mM
233 NaCl treated plants (Fig S2). It should be noted that the growth media used in the current study
234 included 1.2 mM K^+ to support plant growth in all conditions and the ≥50 mM KCl treatments
235 provide excess K^+ beyond its expected range serving as a nutrient (0.1-6 mM) (Ashley et al.,
236 2006). The more tolerant species, *S. parvula*, was more resilient to higher concentrations of KCl
237 than *A. thaliana* before it showed significant defects in both primary and lateral growth (Fig 1B,
238 S3A, and S3B). *S. parvula* root hair length was also less affected compared to that in *A. thaliana*
239 (Fig 1C, S3C). Compared to the same concentration of NaCl treatments, KCl seemed to be more
240 toxic even to the more salt stress-tolerant *S. parvula* (Fig 1A, B, D). These results suggest that
241 despite similar levels of osmotic stress elicited by K^+ and Na^+ at equal concentrations, K^+ may
242 exert additional stresses different from Na^+ that may initiate physiological responses specific to
243 K^+ stress.
244 Because plant growth is tightly coupled to photosynthesis, we tested how the rate of
245 CO_2 assimilation was affected by K^+ toxicity. CO_2 assimilation was reduced in *A. thaliana* in
246 response to 150 mM KCl within 24 hours after treatment (HAT), but *S. parvula* did not show any
247 short-term effects (Fig 1E). Under longer-term treatments, there was a significant reduction in
248 total leaf area in both species and the reduction was more pronounced with high K^+ (Fig 1D).
249 Consequently, in *A. thaliana*, the total carbon content in shoots declined within 72 HAT (Fig 1F).
250 Overall, 150 mM KCl was sufficient to induce physiological stress phenotypes in roots
251 and shoots of *A. thaliana* within a 3-day period, while impacting long-term growth in *S. parvula*
252 (Fig 1 and S2). Notably, 150 mM KCl treatment given for more than a week was lethal to *A.*
253 *thaliana* in all tested growth conditions. Therefore, we selected 150 mM KCl for our cross-
254 species comparative-omics analyses to investigate K^+ toxicity responses, when both species are
255 expected to show active cellular responses to minimize or tolerate stress during the early stages
256 of the treatment at 0, 3, 24, and 72 HAT (Fig S1).

257 **Excess K^+ causes nutrient depletions in *A. thaliana* but not in *S. parvula***

258 Given the role of K as an essential macronutrient, plants have evolved multiple
259 transporters to facilitate entry of K^+ into roots rather than its exit pathways (Shabala and Cuin,
260 2008). Therefore, we first hypothesized that high K^+ in soils will lead to high K^+ contents in

261 plants and shoots will accumulate more of the excess K^+ in the transport sequence from soil-
262 root-shoot. Second, we predict that the differential accumulation of K^+ in roots and shoots will
263 alter many cellular processes and thereby affect transport and retention of other nutrients. To
264 test our hypotheses, we quantified the root and shoot contents of 16 established plant
265 nutrients (K, N, P, Mg, S, Ca, Al, Zn, Co, Ni, Fe, Se, Cu, B, Mn, and Mo) and six toxic elements
266 found in most soils at low concentrations (Fig 2) in hydroponically grown *A. thaliana* and *S.*
267 *parvula*. Nitrogen was measured separately but from the same plant samples (see methods and
268 Fig S1). With ionomic profiling, we aimed to test if (a) K^+ would accumulate in plants as an
269 isolated process decoupled from other element accumulation; (b) high K^+ treatment would
270 cause nutrient imbalances; or (c) it allowed entry of other toxic elements and could indirectly
271 cause toxicity symptoms.

272 We observed three notable trends in how the two species partitioned K between roots
273 and shoots (Fig 2A). First, both species kept higher K^+ levels in shoots than in roots, but the
274 difference between shoots and roots was strikingly larger in *S. parvula* than in *A. thaliana,*
275 under control conditions (*i.e.* 0 HAT before exposure to excess K^+). Second, *A. thaliana* reduced
276 the root K^+ levels by 24 HAT compared to 0 HAT, but was unable to maintain the lower K^+ level
277 with prolonged stress, leading to significantly increased K^+ levels in both roots and shoots by 72
278 HAT. Third, *S. parvula* maintained a significantly lower K^+ content in the roots compared to *A.*
279 *thaliana* throughout the stress treatment even when the root K^+ levels increased over time
280 compared to the control. Importantly, *S. parvula* was able to maintain shoot K^+ levels
281 comparable to the control (Fig 2A). While both species had a higher total K^+ content in shoots
282 than in roots, only *A. thaliana* allowed a further increase in its shoot K^+ content under the
283 current experimental conditions. *S. parvula* appeared to avoid using shoots as a sink for excess
284 K^+ compared to *A. thaliana*.

285 Higher accumulation of K^+ in *A. thaliana* was not an isolated process and it was coupled
286 to a severe nutrient imbalance leading to the depletion of seven nutrients (Fig 2B-D). In line
287 with uninterrupted root growth observed under high K^+ stress (Fig 1A), *S. parvula* did not show
288 a nutrient imbalance. As summarized in Figure 2D, *S. parvula* showed a remarkable capacity in
289 maintaining major macronutrients (C, N, and P) at steady states upon exposure to excess K^+,

290 while in *A. thaliana* all three major nutrients were depleted as K^+ significantly accumulated over
291 time in both roots and shoots.

292 We further observed that excess K^+ did not cause accumulation of any other element
293 that could cause indirect toxicity effects in either species (Fig 2C). Therefore, we can rule out
294 the possibility of observing indirect toxicity effects from other non-nutrients (heavy metals) in
295 downstream analyses (metabolome and transcriptome analyses) to deduce cellular processes
296 affected by excess K^+. Depletion of Na in roots (Fig 2C) in both species indirectly showed the
297 effort by both species to limit the entry of K^+ and/or increase export using K/Na transporters or
298 channels that can act non-selectively on both ions. However, the overall effects on the ionomic
299 profiles indicated that a greater capacity to extrude K^+ from the soil-root interface or prevent
300 entry into the roots from soil cannot be the only major mechanism underlying K^+ toxicity
301 tolerance in *S. parvula*. For example, *S. parvula* showed higher fold-increase of root K upon KCl
302 treatment although the overall K content was still lower than the K content in *A. thaliana* roots
303 (Fig 2A).

304 ***S. parvula* is more responsive than *A. thaliana* at the metabolome level to high K^+ stress**

305 We obtained 472 metabolites of which 145 are known and 327 were unannotated
306 (Table S1) to expand our search to identify cellular processes influencing responses to high K^+
307 stress (Fig 3). Interestingly, we found that *S. parvula* roots, which showed minimal changes at
308 the physiological and ionomic levels compared to *A. thaliana* during high K^+ stress, was more
309 responsive at the metabolomic level (Fig 3A). Considering the higher fraction of unannotated
310 and hence unknown metabolites in metabolite profiles (Table S1), we tested if the unknown
311 metabolite pool had a similar response trend to the known metabolites identified between the
312 two species (Fig 3B). In all tissue/time points, we observed a high correlation of relative
313 abundances of metabolites, whether known metabolites (Fig 3B, r) or all metabolites including
314 unknowns (Fig 3B r’) were considered. For downstream analysis, we only considered the known
315 metabolites with significant abundance changes (abbreviated as MACs for this study) between
316 control and KCl treated conditions (Fig 3A). We further categorized them into (1) amino acids
317 and immediate precursors or derivatives, (2) fatty acids and lipids, (3) nucleic acids, (4) organic

318 acids and their immediate derivatives, and (5) sugars, sugar alcohols, and their associated
319 derivatives (Table S1, Fig 3C).
320 Overall, the metabolic profile comparisons between the two species showed three
321 distinct trends. First, with longer stress durations, the number of MACs increased in all tissues
322 for both species (Fig 3A, C). Second, shoots had more MACs in *A. thaliana*, while *S. parvula*
323 contained more MACs in roots in response to excess K^+ (Fig 3A, C). The higher responsiveness of
324 the shoot metabolome in *A. thaliana* is aligned with our initial hypothesis that we would expect
325 more metabolic disturbances in photosynthetic tissues when excess K^+ accumulated more in
326 shoots (Fig 2A). In contrast, the *S. parvula* root metabolome was more responsive compared to
327 both the metabolomes of *A. thaliana* root and *S. parvula* shoot (Fig 3C), suggesting an
328 alternative response strategy of adjusting predominantly the root metabolites in a species more
329 tolerant to K^+ toxicity. Third, increased abundances of multiple primary metabolite pools
330 especially in *S. parvula* roots (Fig 3D, Root, outer circle) were conspicuous against the overall
331 depletion of primary metabolites in *A. thaliana* in all tissues/time points (Fig 3D, Root and
332 Shoot, middle circle). One of the largest groups that changed in metabolite abundance during
333 high K^+ stress was amino acids and their derivatives in *S. parvula*. Further, sugars and the
334 associated metabolite pools changed in larger proportion in roots of both species and in *A.*
335 *thaliana* shoots. This suggested that the two species primarily used different metabolic
336 groups/pathways to respond to high K^+ stress, a notion further supported by few cross-species
337 overlaps among MACs (Fig 3A). Therefore, we further examined how amino acids and sugars
338 significantly changed from control to high K^+ stress conditions over time.
339 Species specific MACs can indicate metabolic pathways or metabolite groups that are
340 responding to minimize cellular toxicity, severely interrupted by stress, or both. Excess K
341 detrimentally affected *A. thaliana* but hardly interrupted the growth of *S. parvula* (Fig 1).
342 Therefore, we explored the possibility that metabolic pathways or groups represented by MACs
343 in *S. parvula* were enriched in pathways acting towards minimizing cellular stress, while MACs
344 in *A. thaliana* were more representative of pathways or groups disrupted by high K^+ stress.
345 More sugars and amino acids that can serve as osmolytes (raffinose, myo-inositol, sucrose, and
346 proline) (Fig 3D) (Gong et al., 2005) during salt stress increased in *S. parvula* compared to *A.*

347 *thaliana.* When we tested for enriched metabolic pathways or metabolite groups among MACs,
348 galactose metabolism was enriched in *A. thaliana* shoots and *S. parvula* roots (Fig S4A). The
349 metabolites in galactose metabolism (KEGG Pathway ID:ath00052) included several key
350 metabolites (for e.g. galactinol, myo-inositol, and raffinose) (Fig S4B) which are known to
351 protect plants against oxidative and osmotic stresses (Taji et al., 2002; Nishizawa et al., 2008).
352 Interestingly, these increased uniquely in *S. parvula* roots (Fig S4B), suggesting coordinated
353 metabolic adjustments balancing C and N sources to maintain growth while minimizing damage
354 from oxidative bursts in *S. parvula* roots. Overall, the more stress tolerant species, *S.parvula*,
355 seemed to boost the protective metabolite pools while the more stress sensitive species, *A.*
356 *thaliana*, was depleting its initial pools for such protective metabolites during stress.

357 ***A. thaliana* shows wide-ranging misregulation of transcriptional resources during peak stress**
358 **response times reflective of its critical failures to maintain cellular processes**

359 We next examined the transcriptional stress response landscapes and sought to deduce
360 specific cellular processes initiated by *A. thaliana* and *S. parvula* after exposure to high external
361 K^+. Such cellular processes could further build on time-dependent physiological, ionomic, and
362 metabolic processes we identified earlier in this study as responses to excess K^+ accumulation.
363 We obtained 12-23 million reads per RNA-Seq library prepared from three biological replicates
364 of root and shoot samples of both species, harvested at four time points (0, 3, 24, and 72 HAT)
365 (Fig S1). A total of ~70 - 90% reads were uniquely mapped to primary protein-coding gene
366 models in *A. thaliana* (TAIR10) and *S. parvula* (V2.2) reference genomes (Table S2).

367 The Principal Component Analysis (PCA) on shoot and root transcriptomes clustered
368 samples based on the treatment time points with *A. thaliana* showing a greater separation
369 between conditions compared to *S. parvula* (Fig S5A). The individual transcriptomes in pairwise
370 comparisons showed a higher correlation within *S. parvula* samples than for *A. thaliana*
371 samples (Fig S5B). Overall, *S. parvula* had fewer transcriptome-wide changes in response to
372 high K^+ stress than *A. thaliana.* PCA on 23,281 ortholog pairs identified between the two species
373 further supported that *A. thaliana* transcriptomes had a greater variance along a temporal
374 trajectory for duration of exposure to excess K^+, while *S. parvula* showed a similar trajectory but
375 with a much smaller variance (Fig 4A). The total number of differentially expressed genes

376 (DEGs) that showed a significant response in at least one time point was remarkably higher in *A.*
377 *thaliana* (9907 in roots and 12574 in shoots) compared to that in *S. parvula* (1377 in roots and
378 494 in shoots) (Fig S6 and Table S3). This observation led us to question whether the stress
379 sensitive *A. thaliana* is transcriptionally adjusting and concurrently failing to maintain steady
380 levels of critical cellular processes, while the more stress tolerant *S. parvula* is only responding
381 with minimal adjustments to a subset of processes *A. thaliana* may be adjusting suboptimally.
382 Therefore, we first identified the key cellular processes and pathways *A. thaliana* was
383 transcriptionally adjusting, to deduce processes interrupted or misregulated due to excess K^+ as
384 well as processes likely activated for protective roles.

385 We annotated all DEGs with a representative Gene Ontology (GO) function (Table S4, S5,
386 S6) and examined their time dependent progression in *A*. *thaliana* (Fig 4B and S6). The temporal
387 transcriptomic response climaxed at 24 HAT as shown by having the highest number of DEGs
388 and the largest number of enriched cellular functions. Additionally, the shoots lagged behind
389 the root responses (Fig 4B). This lag is reflected by the most number of DEGs and enriched
390 functions observed during 3-24 HAT in roots and 24-72 HAT in shoots. Despite the response
391 time lag, the enriched processes are largely shared between roots and shoots in *A. thaliana* (Fig
392 4B).

393 One of the most emergent cellular process categories enriched in both roots and shoots
394 in *A. thaliana* was response to stress (Fig 4B). Within this category, the prevalent specific
395 responses across all time points were responses to salt, oxidative, and ionic stresses.
396 Unexpectedly, biotic stress-related GO terms (e.g. response to bacterium, response to chitin,
397 and immune response) were also prominently enriched at all time points (Fig 4B). Induction of
398 biotic stress responses in *A. thaliana* seemed counterintuitive when the *S. parvula* orthologs of
399 these *A. thaliana* high K^+-induced DEGs were mostly suppressed in response to high K^+ stress
400 (Table S3 and S7). Given that *A. thaliana* shows a peak transcriptional response at 24 HAT, this
401 made us question whether we were observing transcriptional chaos rather than targeted
402 transcriptional resource allocation between biotic and abiotic stresses to manage the extant
403 stress experienced by *A. thaliana*.

404 We observe three indicators to suggest that there is overall misregulation in critical
405 signaling pathways that highlight chaotic and inefficient responses to overcome cellular toxicity
406 intensified due to excess K^+ accumulation in *A. thaliana* (Fig 2). First, the cellular response to
407 stress in shoots included enriched functions representing all major plant hormone pathways
408 (Fig 4B). In addition to the ABA response enriched at all time points, all other major plant
409 hormone responses are elicited concurrently during 24-72 HAT in shoots in the absence of
410 canonical developmental or biotic stress cues, suggesting disruptions in hormone signaling.
411 Second, we find autophagy as the most enriched process with the highest proportion of DEGs
412 (24 DEGs or 60% of all annotated, adjusted p-value 9.39E-07), accompanied by additional
413 processes including cell death and leaf senescence, enriched during 24-72 HAT in shoots. Third,
414 we see enriched responses to cold, heat, wounding, drought, and hypoxia which all share
415 common genetic mechanisms with responses to oxidative stress also prevalent during 24-72
416 HAT (Fig 4B). This suggested unmitigated oxidative stresses. We compared the ROS scavenging
417 capacity between *A. thaliana* and *S. parvula* leaves during high K^+ stress, by assessing the
418 accumulation of oxidative stress markers, H_2O_2 and O_2^-. As predicted by the transcriptional
419 response, leaves of *A. thaliana* showed greater levels of oxidative stress compared to *S. parvula*
420 (Fig 4C). While the reduced numbers of DEGs at 72 HAT especially in roots indicated a degree of
421 acclimation in *A. thaliana* (Fig 4B and S6B), the prolonged ABA signaling together with non-
422 specific activation of hormone pathways, autophagy, and oxidative stresses serve as molecular
423 phenotypes that indicate erratic and inefficient responses especially in *A. thaliana* shoot, which
424 could lead to eventual failures in cellular homeostasis after prolonged exposure to high K^+
425 stress as supported by the observed growth phenotypes (Fig 1). These molecular phenotypes
426 become even more compelling when compared to their respective transcriptional profiles in *S.*
427 *parvula* orthologs which remained mostly unchanged (Fig 4D).
428 Primary metabolic processes involving carboxylic acid/carbohydrate and amino acid
429 metabolism form the second largest group among the most affected transcriptional categories
430 following stress responses (Fig 4B). These processes were enriched in all time points during high
431 K^+ stress in both *A. thaliana* roots and shoots. This further supports the previous physiological
432 and metabolic responses that showed primary C and N metabolism pathways were severely

433 affected (Fig 1E and F, Fig 3C and D). Notably, most transcriptional adjustments to C and N
434 metabolism were detected at later time points. For example, interruptions to photosynthesis at
435 24 and 72 HAT (Fig 1E) were aligned with the corresponding transcriptional processes enriched
436 at the same time points in *A. thaliana* shoots (Fig 4B). On the contrary, growth responses
437 influenced by nutrient homeostasis during stress, such as root development, was detected as a
438 transcriptionally enriched process early at 3 HAT (Fig 4B), although the interruptions to root
439 hair growth was detected later at 72 HAT (Fig 1C).

440 ***S. parvula* shows a confined yet a targeted transcriptomic response steered towards stress**
441 **tolerance while supporting enhanced C-N metabolism**

442 We searched for DEGs among *A. thaliana* whose *S. parvula* orthologs also showed active
443 responses (Fig 5A). These ortholog pairs likely represent cellular processes that require active
444 transcriptional adjustments to survive the accumulation of excess K^+ in plant tissues even in a
445 more stress tolerant species. We predicted that the transcriptional adjustments in diametric
446 responses (*i.e.* genes that are induced in one species when their orthologs are suppressed in
447 the other species) between the species will be detrimental to the stress sensitive species, while
448 shared responses in similar directions will be beneficial yet likely underdeveloped or
449 unsustainable to survive the stress by the stress sensitive species. There were fewer ortholog
450 pairs showing diametric responses (256 and 60 ortholog pairs in roots and shoots, respectively)
451 compared to those with shared responses (305 and 283 in roots and shoots respectively)
452 between *A. thaliana* and *S. parvula* (Fig 5A, S6).

453 Among the diametric responses, the largest functional cluster identified as induced in *A.*
454 *thaliana*, while suppressed in *S. parvula* roots was response to stress (Fig S6A). Most of the
455 subprocesses in this cluster are associated with biotic stress (Table S9). Therefore, we further
456 assessed this transcriptional divergence between the two species as a proportional effort
457 invested in biotic vs abiotic stress responses out of the total DEGs responded in at least one
458 time point within each species (Fig 5B). The effort to suppress biotic stress responses in *S.*
459 *parvula* roots (10%) was similar to the proportional induction for biotic stress responses in *A.*
460 *thaliana* (9%) within total non-redundant DEGs (Fig 5B). Contrarily, orthologs that were
461 suppressed in *A. thaliana*, but induced in *S. parvula* roots were associated with ion transport

462 and cell wall organization (Fig S6A). These transcriptional adjustments support the physiological
463 response in *S. parvula* where new roots grew uninterrupted maintaining ion uptake during
464 exposure to excess K^+, compared to *A. thaliana* roots that failed to keep nutrient uptake and
465 subsequently stopped growing (Fig 1B and 2C). In shoots, orthologs induced in *A. thaliana* but
466 suppressed in *S. parvula* include multiple genes associated with defense responses,
467 corroborating our observation of the erratic transcriptional resource allocation to biotic stress
468 responses in *A. thaliana* (Fig S6B). The orthologs suppressed in *A. thaliana* but induced in *S.*
469 *parvula* shoots were enriched in carboxylic acid and amine metabolism and associated
470 transport functions (Fig S6B). This reflects the transcriptional undertaking in *S. parvula* that
471 supports continued growth (Fig 1B, D, E, and S2), upheld nutrient balance (Fig 2B, C, and D), and
472 induction of metabolite pools associated with C and N metabolism (Fig 3C, D) during high K^+
473 stress, while *A. thaliana* shows opposite physiological, ionomic, and metabolic responses.
474 The ortholog pairs that showed shared induction (156 and 199 in root and shoot,
475 respectively) in *A. thaliana* and *S. parvula* were largely represented by abiotic stress responses
476 mediated by hormones including ABA (Fig S6 and Table S10). The ortholog pairs with shared
477 suppression (149 and 84 in root and shoot, respectively) were enriched in functional processes
478 involved in biotic stress in roots and photosynthesis in shoots. Therefore, at least in roots, *A.*
479 *thaliana* seems to actively reduce its transcriptional allocation to biotic stress via subsets of
480 genes regulated congruently with *S. parvula* (Fig S6A). However, genes showing this pattern
481 were negligible based on a proportional effort (0.004% in *A. thaliana*) to reduce transcriptional
482 allocation to biotic stress responses compared to *S. parvula* (10%) in roots (Fig 5B).
483 Over 50% of orthologs differently expressed in response to excess K^+ in *S. parvula* roots
484 and ~30% in shoots show unique expression trends different from *A. thaliana* (Fig 5A). Both *S.*
485 *parvula* specific responses and diametric responses between the two species were more
486 pronounced in roots than in shoots. We predicted that *S. parvula* activates decisive
487 transcriptional regulatory circuits that are either absent (*i.e. S. parvula*-specific responses) or
488 wired differently (*i.e.* diametric responses) in roots than in shoots when responding to excess K^+
489 stress.

490 The overall transcriptomic response of *S. parvula* encapsulates induction of more
491 targeted salt stress responses compared to *A. thaliana*, including especially oxidative stress
492 responses, sugar and amino acid metabolism, and associated ion transport, with concordant
493 induction in growth promoting processes and transcriptional resource recuperation by
494 suppressing biotic stress responses (Fig 5C). The transcriptional effort to facilitate growth
495 amidst excess K^+ accumulation in tissues is reflected by induced transcripts involved in cell wall
496 biogenesis, RNA processing, and development along with concurrent suppression for rapid
497 growth limiting processes such as cell wall thickening and callose deposition (Table S10).

498 **Differential expression of K^+ transporters lead to differential compartmentalization of excess**
499 **K^+ concurrent to extensive stress signaling cascades triggered in *A. thaliana***

500 Our ionome profile comparisons demonstrated that *A. thaliana* exposed to high external
501 K^+ over time accumulate K^+ in its tissue concurrently with the depletion of C, N, and P at a
502 whole plant level (Fig 2). Additionally, transcriptional responses to excess K^+ had ion transport
503 among the most represented functions within and between species comparisons (Fig 4B, 5C,
504 and S6A). The ability in *S. parvula* to curb K^+ accumulation and prevent the depletion of major
505 nutrients led us to hypothesize that K^+ transporters are differentially expressed in the two
506 species as a first line of defense against a severe nutrient imbalance during excess K^+ stress.
507 Among over 70 transporters reported to transport K^+ in *A. thaliana* (Shabala and Cuin, 2008),
508 we predicted that the transcripts coding for K^+ transporters which allow K^+ into roots and
509 upload K^+ into the xylem or phloem would be primary targets for down-regulation in the effort
510 to restrain K^+ accumulation. On the other hand, transcripts sequestering K^+ into the vacuoles,
511 especially when tissue [K^+] is high, will be induced. To assess these predictions, we checked the
512 transcript profiles of all known K^+ transporters.

513 We first searched for K^+ transporter transcripts that showed significantly different basal
514 level abundances (Fig 6A) and responses to high K^+ stress (Fig 6B) between *A. thaliana* and *S.*
515 *parvula*. We categorized four transport routes that would limit accumulation of K^+ in plants and
516 compartmentalize excess K^+ within tissues or cells: a. limit entry into roots, b. promote efflux
517 from roots, c. constrain long distance transport between root and shoot, and d. enhance
518 sequestration into vacuoles. We then sought to find out routes that are potentially failing to

519 keep up with the mounting stress in *A. thaliana* and/or more strategically exploited by *S.*
520 *parvula*.
521 **a. Limit entry into roots.** The most suppressed gene in *A. thaliana* under excess K^+ stress
522 is the *high-affinity K^+ transporter 5* (*HAK5*) that showed a 13-fold reduction at 24 and 72 HAT. At
523 low soil K^+ levels, the major transporter for K^+ uptake in roots is HAK5. This mode of K^+
524 transport switches to low affinity transport mediated by the K channel AKT1 that requires the
525 channel subunit KC1 to function at sufficient K^+ levels in soil (Gierth et al., 2005; Xu et al., 2006;
526 Wang et al., 2016) These two major transporters are activated post-translationally by the
527 protein kinase complex calcineurin B-like proteins 1 and 9 (CBL1&9)/CBL-interacting protein
528 kinase 23 (CIPK23) (Ragel et al., 2015). Under excess K^+ stress both transport complexes and
529 their core post-translational regulatory unit in *A. thaliana* roots are suppressed (Fig 6B, C, and
530 S7A). The transcripts coding for the transporters are unchanged in *S. parvula* roots but the
531 interacting partners of the kinase complex are suppressed (Fig 6B and S7A). The transcriptional
532 effort to limit entry of K^+ into roots during high K^+ stress is further exemplified by the
533 suppression of *RAP2.11*, a transcriptional activator of *HAK5* (Kim et al., 2012) and the induction
534 of *ARF2*, a repressor of *HAK5* transcription (Zhao et al., 2016), in *A. thaliana* roots (Fig 6C).
535 Similarly, *ARF2* is also induced in *S. parvula* roots. Other K^+ transporters that are reported to
536 function in K^+ uptake into roots are also suppressed in *A. thaliana* (e.g. KUP6 and KUP8) under
537 excess K^+ stress (Fig 6B). While a similar transcriptional suppression for KUP transporters is
538 absent in *S. parvula* roots*,* it shows concerted transcriptional suppression of cyclic nucleotide
539 gated channels, *CNGC3/*10/12/13 (Fig 6B and C), suggesting down-regulation of non-selective
540 uptake of monovalent cations including K^+ into roots (Gobert et al., 2006; Guo et al., 2008).
541 **b. Promote efflux from roots.** We do not know of any K^+ efflux transporter that
542 functions to extrude excess K^+ from roots back to the soil under excess K^+ conditions. However,
543 *S. parvula,* which has evolved in soils naturally high in K^+, induced transcription of a K^+ outward
544 rectifying channel, *GORK* (Ivashikina et al., 2001) and the Na^+ exporter *SOS1* (Shi et al., 2000) in
545 roots (Fig 6B, C and S8A). Induction of *GORK* is known to cause K^+ leakage from roots under
546 biotic and abiotic stresses in plants leading to programmed cell death (Demidchik et al., 2014).
547 We propose that *S. parvula* has evolved to allow export of excess K^+ via induction of GORK

548 without the destructive downstream consequences of cell death as expected in *A. thaliana* (Fig
549 6B, C, 4B, and 4D). We also note that the basal expression level of *GORK* in *S. parvula* roots is
550 higher than in *A. thaliana* roots (Fig 6A). Next, SOS1, the antiporter with the highest Na^+ efflux
551 capacity in roots, is known for its Na^+ specificity (Oh et al., 2009). Therefore, induction of *SOS1*
552 in *S. parvula* under high K^+ stress (Fig S8A) is likely an effort to counterbalance the increasing
553 osmotic stress due to elevated K^+ by exporting available Na^+ from roots. This explanation fits
554 with Na^+ being the only ion depleted in *S. parvula* roots during excess K^+ stress (Fig 2C).
555 Similarly, a well-documented Na^+/K^+ transporter family in plants encoded by *HKT1* (Uozumi et
556 al., 2000; Ali et al., 2016) known for its key roles in minimizing Na-induced salt stress, is present
557 as a single copy (AtHKT1) for selective Na^+ transport in *A. thaliana*. In *S. parvula*, among the two
558 duplicated *HKT1* paralogs, *SpHKT1;2* has been demonstrated to show selective-K^+ transport
559 while Sp*HKT1;1*, orthologous to *A. thaliana HKT1,* shows selective-Na^+ transport (Ali et al.,
560 2018). We observe basal-level expression biases for the *S. parvula HKT1* paralogs, however the
561 K^+-selective paralog, despite its much higher transcript abundance, did not significantly respond
562 to excess K^+ (Fig S8B).

563 **c. Constrain long distance transport between root and shoot.** The long-distance
564 transport of K^+ via xylem loading is mediated by SKOR, NRT1.5, and KUP7 in *A. thaliana*
565 (Gaymard et al., 1998; Han et al., 2016; Li et al., 2017). *SKOR* and *NRT1.5* were suppressed in *A.*
566 *thaliana* roots as predicted. However, *KUP7* showed induction in *A. thaliana* roots at 72 HAT
567 concordantly when K^+ accumulation was observed in shoots following exposure to high K^+ (Fig
568 6B and 2A). Contrastingly, none of these transporters were differently regulated in *S. parvula*
569 roots. AKT2 is the dominant channel protein regulating long distance transport via loading and
570 unloading to the phloem (Dreyer et al., 2017). It too is significantly suppressed in *A. thaliana*
571 shoots, but unchanged in *S. parvula* roots and shoots (Fig 6B and C).

572 **d. Enhance sequestration into vacuoles.** Vacuolar K^+ concentration can fluctuate widely,
573 and this sequestration capacity is tightly controlled with pH of the vacuole primarily regulated
574 by the Na^+,K^+/H^+ antiporters, NHX1 and NHX2. These are spatiotemporally regulated with
575 overlapping functions. Additionally, NHX4 is a more selective K^+/H^+ antiporter functioning to
576 store K^+ in vacuoles at a smaller scale (Bassil et al., 2019). In *A. thaliana* during high K^+ stress,

577 *NHX2* is induced in roots, whereas *NHX1* is induced in shoots. However, the transcriptional
578 signal to promote K^+ sequestration in *A. thaliana* either in roots or shoots is unclear, because in
579 roots *NHX1* is suppressed while in shoots *NHX4* is suppressed (Fig 6B and C). This tissue-specific
580 mixed regulatory pattern observed in *A. thaliana* is absent in *S. parvula*. Nonetheless, *S. parvula*
581 does not show any pronounced transcriptional commitment to enhance transport of excess K^+
582 into vacuoles in shoots. The nonselective slow-activating vacuolar (SV) channel encoded by
583 *TPC1* (tandem-pore calcium channel) and K^+-selective vacuolar channels (TPK/KCO) play primary
584 roles in regulating the release of K^+ into the cytosol from the vacuole (Voelker et al., 2006;
585 Gobert et al., 2007). Under high K^+ stress, *A. thaliana* induces *KCO6* in roots while keeping *TPC1*
586 unchanged. However, *S. parvula*, through suppression of *KCO5*, seems to attempt to
587 preferentially retain excess K^+ sequestered in vacuoles in roots (Fig 6B and C). Such an attempt
588 to compartmentalize excess K^+ in vacuoles is further suggested by the suppression of tonoplast
589 localized nonselective cation channels *CNGC19* and *CNGC20* (Yuen and Christopher, 2013) in *S.*
590 *parvula* roots.

591 Our initial physiological assessments showed that photosynthesis was decreased at 24
592 HAT in *A. thaliana* (Fig 1E). The transcriptional signal of K^+ transporters associated with
593 maintaining turgor of guard cells corroborate the physiological observation, by showing a bias
594 towards closed stomata via an induction of *GORK* coordinated with a suppression of guard cell
595 localized *KAT1/2* in *A. thaliana* shoots (Fig 6B and C) (Ivashikina et al., 2001; Szyroki et al.,
596 2001). The comparable regulatory unit for closed stomata is not induced in *S. parvula* shoots as
597 a transcriptomic signal.

598 Osmotic and oxidative stresses combined in plant tissues entail regulation of water
599 transport mediated by aquaporins and multiple signaling cascades regulated by calcium
600 signaling pathways (Srivastava et al., 2014; Takahashi and Shinozaki, 2019). Accumulation of
601 excess K^+ leads to a sweeping array of differentially regulated aquaporins and calcium signaling
602 pathway genes in both roots and shoots of *A. thaliana* compared to a limited regulation
603 detected for *S. parvula* (Fig S7). This reinforces our overall depiction of the stress response in *S.*
604 *parvula* to reflect a restrained set of transcriptional responses during excess K^+ stress.

605 **Excess K^+ induced nitrogen starvation and failure to activate key pathways in N-metabolism**
606 **are critical flaws in *A. thaliana* compared to *S. parvula***
607 The steep drop in total N content in *A. thaliana* compared to *S. parvula* (Fig 2B and D);
608 reduction in amino acids and derivatives in *A. thaliana* while these metabolites increased in *S.*
609 *parvula* (Fig 3C and D); followed by suppression of transcriptomic signals associated with amine
610 metabolism in *A. thaliana* when these were induced in *S. parvula* (Fig 4B, 5C, and S6B)
611 necessitated further examination on how excess K^+ may alter N-metabolism in plants. Under
612 low soil K levels, N uptake in the form of nitrate is tightly coupled to K uptake and translocation
613 within the plant. Many of the K and N transporters or their immediate post-transcriptional
614 activators are co-regulated at the transcriptional level (Coskun et al., 2017). We searched for
615 specific transcriptomic cues to determine how N transport was disrupted under high K^+, leading
616 to a deficiency in physiological processes needed to maintain growth and development or a
617 shortage of protective metabolites against oxidative and osmotic stress initiated by excess K^+ in
618 tissues.
619 Does excess K^+ induce N starvation in *A. thaliana*? The dual affinity nitrate transporter,
620 NRT1.1 (NPF6.3/CHL1) is the main NO_3^- sensor in plant roots in addition to accounting for up to
621 80% of NO_3^- uptake from roots (Feng et al., 2020). Within 3 HAT and onwards, *NRT1.1* in *A.*
622 *thaliana* roots is down-regulated (Fig 7A). At low soil NO_3^- levels, *NRT1.1* is activated by *CIPK23*
623 to function as a high affinity NO_3^- transporter (Coskun et al., 2017). We note that in *A. thaliana*
624 (and not in *S. parvula*) roots, *CIPK23* is concurrently suppressed with the main K uptake system
625 formed of *HAK5* and *AKT1-KC1* (Fig 6C). This potentially limits the N content in roots within 24
626 HAT (Fig 2B) and we see *A. thaliana* roots activating N starvation signals by inducing the
627 expression of high affinity NO_3^- transporters, *NRT2.1* and *NRT2.4* upon high K^+ treatment (Fig
628 7A) even when the growth medium in the current experimental condition has sufficient NO_3^-
629 levels. NRT2.1 and NRT2.4 account for over 75% of influx when soil NO_3^- levels are low (O'Brien
630 et al., 2016).
631 The long-distance transport from root to shoot via xylem loading of NO_3^- in roots is
632 primarily regulated via NRT1.5 (NPF7.3) which is a NO_3^-/K^+ cotransporter (Li et al., 2017). We
633 observe that in *A. thaliana* (and not in *S. parvula*) roots, *NRT1.5* is suppressed possibly in an

634 attempt to limit excess K^+ accumulation in shoots, but consequently depriving NO_3^- in shoots
635 (Fig 2B and 7A). This high K^+ induced N starvation environment generated in *A. thaliana* is
636 further reflected by its additional transcriptional effort to remobilize NO_3^- internally. For
637 example, *NRT1.7* and *NRT1.8* are induced to promote translocation of NO_3^- from old to young
638 leaves and from xylem back into roots respectively, while *NRT1.9, NRT1.11,* and *NRT1.12* are
639 suppressed to restrict transport via phloem and limit NO_3^- movement in shoots under low NO_3^-
640 levels (Fig 7A) (O'Brien et al., 2016). The transcriptional regulatory emphasis on *NRT1.8* is
641 outstanding during excess K^+ stress, given that it is the highest induced (104-fold and 73-fold at
642 24 and 72 HAT, respectively) in the entire *A. thaliana* transcriptomic response (Fig 7A and Table
643 S3). Even in *S. parvula* which has overall a more restrained transcriptomic response, an ortholog
644 copy of *AtNRT1;8* is induced in roots at 24 HAT. Additionally, *NRT1.8* is triplicated in *S. parvula*
645 (Oh and Dassanayake, 2019), allowing additional regulatory flexibility to the species to
646 redistribute NO_3^- via the xylem back to the roots.
647 NH_4^+ provides the second major source of N following NO_3^- and the growth medium
648 provided in the current experimental conditions includes NH_4^+ at 0.2 mM compared to 1.4 mM
649 NO_3^-. Therefore, we expected to see an induction in NH_4^+ transporters as an alternative N
650 nutrition response to overcome the high K^+-induced N-starvation, primarily caused through the
651 co-suppression of NO_3^- and K^+ uptake, in *A. thaliana* roots. However, there is a widely
652 documented reciprocal antagonistic activity between NH_4^+ and K^+ transport contrasting to the
653 interdependent cotransport activity between NO_3^- and K^+. Excess NH_4^+ limits root uptake of K^+
654 and its translocation to shoots and an external supply of K^+ or induction of K^+ transporters
655 relieves ammonium toxicity (Coskun et al., 2017). Further, the high affinity NH_4^+ specific
656 ammonium transporters (AMT) are inhibited by CIPK23 when the same is known to activate
657 NO_3^- and K^+ transporters (Straub et al., 2017). Nonetheless, the antagonistic transport functions
658 between NH_4^+ and K^+ are not established under excess K^+ and non-toxic NH_4^+ levels.
659 Counterintuitive to our expectations, *AMT1;1/2/3*, which encode transporters that account for
660 >90% of high-affinity ammonium uptake into roots (Yuan et al., 2007), were co-suppressed in *A.*
661 *thaliana* concurrent to suppression of K^+ transporters that regulate soil to root influx upon
662 excess K^+ (Fig 7A). The exception to this coordinated suppression was seen with *AMT1;5* which

663 was induced upon high K^+ in *A. thaliana* roots (Fig 7A). Notably, *AMT1;5* has been shown to
664 have an opposite activation mode compared to the other *AMTs* (Neuhauser et al., 2007).
665 We next checked whether the N assimilation pathway from NO_3^- to glutamine via NH_4^+
666 was also suppressed in *A. thaliana* experiencing a high K^+-induced N-starvation. Indeed, the
667 genes coding for nitrate reductase (*NIA1/NR1, NIA2/NR2*) and nitrite reductase (*NIR*) were
668 coordinately down-regulated in *A. thaliana* root and shoot under high K^+ (Fig 7B). In
669 angiosperms including *A. thaliana*, the main assimilation point of inorganic N to organic
670 compounds is the GS-GOGAT (glutamine synthetase-glutamate synthase) pathway which is
671 tightly coupled to the N and C metabolic state of the plant (O'Brien et al., 2016). The GS enzyme
672 coded by the *GLN* family uses NH_4^+ derived from primary N uptake; recycled from
673 photorespiration; or remobilized from protein hydrolysis. The GOGAT enzyme comprises
674 plastid-targeted *GLU* and cytosolic *GLT* to form a net output of glutamate from glutamine and
675 2-oxoglutarate, which can be converted to various amino acids and organic acids (O'Brien et al.,
676 2016; Ji et al., 2019). The cytosolic *GLN1;2* and plastidial *GLN2* (coding GS enzymes) together
677 with *GLT* and *GLU1* (coding GOGAT enzymes) were suppressed under a low N and C metabolic
678 environment created by excess K^+ (Fig 2D and 7B). Contrastingly, the induction of *GLN1;1* and
679 *GLN1;3* together with *GLU2* especially in *A. thaliana* shoots likely reflects the transcriptional
680 effort to recycle N under a high K^+-induced N-starved condition (Fig 7B).
681 We predicted that the suppression of the overall N-assimilation pathway would be
682 reflected in the change in primary metabolite pools derived from glutamate in *A. thaliana*
683 during excess K-induced N starvation. In our comparative transcriptome profiling, *S. parvula*
684 boosted its transcriptional resource allocation to defend against osmotic and oxidative stresses
685 while *A. thaliana* showed a setback in similar transcriptional efforts (Fig 5B, C and S6). We
686 wanted to see if this setback in *A. thaliana* to mount appropriate defenses against osmotic and
687 oxidative stress coincided with the depletion of metabolites directly derived from glutamate
688 that are known to function as organic osmolytes and antioxidants. Proline is a primary
689 metabolite with dual functions serving as an osmoprotectant and an antioxidant (Hayat et al.,
690 2012). We observed a coordinated effort to accumulate proline and its immediate precursors in
691 the induction of transcripts coding for the key proline biosynthesis enzymes (Fig 7B, *P5CS1/2*) in

692 both species. However only *S. parvula* was able to significantly accumulate proline during
693 exposure to excess K^+ (Fig 7C). We see similar pronounced efforts in increasing antioxidant
694 capacity via GABA and beta-alanine (Fig 7B and C), concordant to increasing synthesis towards
695 raffinose and myo-inositol only in *S. parvula* (Fig S4B) to protect against osmotic stress. Overall,
696 *S. parvula* is not hindered in its capacity to accumulate carbon and nitrogen-rich antioxidants
697 and osmoprotectants by maintaining N uptake from roots and N-assimilation pathways
698 separated from the suppressed K-uptake pathways. Contrastingly, the two processes were
699 jointly suppressed in *A. thaliana* leading to the depleted N resources (Fig 2B) and, in turn,
700 failure to accumulate C and N-rich protective metabolites (Fig 7C).

701 **Co-expressed gene clusters between *S. parvula* and *A. thaliana* indicate stress preparedness**
702 **in *S. parvula***

703 Given the more targeted transcriptomic responses (Fig 5) and its niche adaptations to
704 survive high K^+ levels found in its native habitat (Oh et al., 2014), we predicted that, in *S.*
705 *parvula*, a large proportion of stress adapted transcripts would be constitutively expressed, as
706 previously reported for stress preparedness at the basal level for B toxicity (Wang et al., 2021).
707 To deduce constitutively expressed transcripts in *S. parvula* with decisive roles in preadaptation
708 toward high K^+, we generated co-expressed ortholog pair clusters using 14,318 and 14,903
709 ortholog pairs expressed in root and shoot respectively, in *A. thaliana* and *S. parvula*. Among
710 them, we identified five root and three shoot co-expressed clusters (Fig 8, RC1-5 and SC1-3,
711 respectively) that had significant basal expression differences and high K^+ stress transcriptomic
712 responses significantly regulated only in one of the species, a pattern that may signify stress-
713 prepared transcriptomes unique to each species (Fig 8 and Table S11).

714 In three out of five root co-expression clusters, only *A. thaliana* orthologs showed
715 induction or suppression with a maximum response at 24 HAT (Fig 8A, RC1-3). These clusters
716 largely represented transcripts associated with stress responses, C and N metabolism,
717 transport, and root development we discussed earlier (Fig 4). Interestingly, the 4th and 5th
718 clusters (Fig 8A, RC4-5) of which *S. parvula* showed a response, accounted for 203 ortholog
719 pairs. Yet, 37% of these orthologs had no functional annotations that could be deduced from
720 Gene Ontologies and therefore could not be meaningfully summarized into representative

721 processes. This highlights the extent of functional obscurity or novelty of genes that respond to
722 specific ionic stresses even in *A. thaliana* (Fig 8A, RC5), and the novel regulatory modes
723 detected in orthologs of closely related species whose functional assignment may have been
724 overlooked due to the lack of responses in the model plant *A. thaliana* (Fig 8A, RC4). In all three
725 shoot co-expressed clusters, *A. thaliana* showed a response that peaked at 24 HAT, while the *S.*
726 *parvula* orthologs showed a constitutive expression either lower than the basal level in *A.*
727 *thaliana* (Fig 8B, SC1), higher than the induced level in *A. thaliana* (Fig 8B, SC2), or equaled the
728 control (0 HAT) level in *A. thaliana* (Fig 8B, SC3). The enriched functions in shoot clusters largely
729 overlapped to include stress responses and C and N metabolic processes. In all, 9836 ortholog
730 pairs, all clusters except RC4 and RC5, showed constitutive expression in *S. parvula* while only
731 76 ortholog pairs (RC4) showed a unique response from *S. parvula* when *A. thaliana* showed
732 constitutive expression (Fig 8). Overall, these co-expressed clusters between *A. thaliana* and *S.*
733 *parvula* demonstrate the stability in transcriptional resource allocation (*i.e.* stress
734 preparedness) in *S. parvula* to facilitate growth and development during excess K^+ stress, while
735 significant alterations are observed for *A. thaliana* orthologs coinciding with its growth
736 interruptions during high K^+ stress and erratic transcriptional resource management.
737

738 **Discussion**

739 Salt stress mechanisms induced by high K^+ are largely unknown compared to the
740 collective understanding for high Na^+ tolerance in plants. Our results demonstrate that high K^+
741 is more detrimental to plants than Na^+ given at the same external concentrations (Fig 1).
742 Previous studies support this observation noting that excess KCl caused more severe salt stress
743 symptoms than NaCl in multiple crops and even among halophytes (Eijk, 1939; Ashby and
744 Beadle, 1957; Eshel, 1985; Matoh et al., 1986; Cramer et al., 1990; Wang et al., 2001; Ramos et
745 al., 2004; Richter et al., 2019). Generally, halophytes have evolved to survive high levels of Na
746 and the subsequent toxicity symptoms entailing oxidative, osmotic, and ionic stresses, while
747 being able to take up K (Kazachkova et al., 2018; Pantha and Dassanayake, 2020). However, the
748 canonical adaptations described for salt tolerance mechanisms associated with NaCl-induced

749 salt stress (Pantha and Dassanayake, 2020) are insufficient to explain adaptations required for
750 KCl-induced salt stress.

751 The molecular mechanisms underlying K^+ toxicity, excess K^+ sensing, and how those
752 signals are transduced to manage overall stress avoidance or mitigation have been poorly
753 investigated in plants. The extremophyte model, *S. parvula,* amidst high K^+ at unfavorable
754 growth levels can sustain its growth and development; compartmentalize excess K more in
755 roots than in shoots; maintain uninterrupted nutrient uptake; increase its antioxidant and
756 osmoprotectant pools; decouple transcriptional regulation between K and N uptake; and
757 coordinately induce abiotic stress response pathways along with growth promoting pathways
758 (Fig 9). Contrastingly, the more stress-sensitive plant, *A. thaliana*, shows interrupted root and
759 shoot growth; excessive accumulation of K^+ in both roots and shoots; depletion of essential
760 nutrients; depletion of N-containing primary metabolites; and sweeping transcriptomic
761 adjustments suggesting initiation of autophagy, ROS accumulation, response to both abiotic
762 and biotic stresses, and responses to all major hormone pathways (Fig 9). We propose two
763 deterministic steps in the overall stress response sequence to survive high K^+ stress.

764 **Surviving high K toxicity by avoiding N starvation**

765 Unlike in *A. thaliana,* even when excess K^+ was accumulating in *S. parvula* roots over
766 time, the overall root growth was not severely affected and nutrient balance was maintained
767 (Fig 1 and 2). Halophytes are known for their ability to maintain nutrient balance and prevent
768 excess salt from accumulating in shoots under salt stresses exerted by NaCl (Kazachkova et al.,
769 2018; Zhao et al., 2020). However, unlike Na, K is a macronutrient and plants have evolved
770 many more functionally redundant transporters to take up K^+ into roots and redistribute into
771 shoots via xylem and phloem (Shabala and Cuin, 2008). When external K^+ levels exceed
772 physiologically optimal conditions, it is not surprising that the immediate response from both
773 plants was to suppress expression of selective K^+ transporters that primarily control K^+ influx
774 from the root soil interface (Fig 6). Additionally, *S. parvula* down-regulates non-selective CNGC
775 cation channels that may be permeable to K^+ especially in roots. Several CNGC type channels
776 are reported to allow Na^+ or K^+ transport and have been implicated in their functions during Na-
777 induced salt stress by controlling Na influx into roots. However, their functional and

778 spatiotemporal specificity remains largely unresolved (Dietrich et al., 2020) and needs to be
779 determined before evaluating how selected CNGCs may be involved in also limiting excess K
780 flow into roots under K-induced salt stress.

781 Concurrent to suppression of K^+ uptake, *A. thaliana* co-suppresses long distance
782 transport of K^+. One of the key transporters used in this process is NRT1.5 which is a co-
783 transporter of NO_3^- and K^+ (Li et al., 2017). NO_3^- is transported as a counterion with K^+ in plant
784 root to shoot translocation as described by the 'Dijkshoorn–Ben Zioni model' (Dijkshoorn et al.,
785 1968; Zioni et al., 1971; Coskun et al., 2017). The suppression of *NRT1.5* limits NO_3^-
786 remobilization in plants (Chen et al., 2012). This obstruction to N transport within the plant is
787 compounded by the transcriptional co-suppression of NRT and AMT transporters known to
788 operate at the root soil interface limiting N intake into plants (Fig 7) (Tegeder and Masclaux-
789 Daubresse, 2018). This creates an N-starved condition for *A. thaliana* not observed for *S.*
790 *parvula.* During limiting K^+ conditions, N-uptake is down regulated to prevent excess N-induced
791 toxicity in plants as a favorable mechanism to adapt to K^+ starvation (Armengaud et al., 2004).
792 This interdependent between N and K transport and regulation that is favorable at low K^+ levels
793 appear to be detrimental at high K^+ levels as it functions as an antagonistic pleiotropic effect
794 (condition dependent traits that can cause positive as well as negative impacts).

795 We observed a significant transcriptional induction of *NRT1.8/NPF7.2* (the most induced
796 gene in *A. thaliana* during excess K^+ stress) in *A. thaliana* and thereby avoid N depletion in roots
797 by N-reimport from the stele (Li et al., 2010). However, this transcriptional effort did not
798 cascade to the ionomic level (Fig 2B and D). N remobilization via induction of *NRT1.8* while
799 concurrently suppressing *NRT1.5* (Fig 7A) during N starvation is regulated by ethylene-jasmonic
800 acid signaling together with low N-sensing by nitrate reductase (Chen et al., 2012; Zhang et al.,
801 2014). Both ethylene and jasmonic acid signaling are among the enriched differently regulated
802 transcriptional processes in *A. thaliana* (Fig 4B). Interestingly, *S. parvula* appears to have a more
803 flexible and effective regulatory capacity to allow N-uptake decoupled from restricted K-uptake
804 and also it does not suppress internal remobilization of NO_3^- and K^+ via NRT1.5 (Fig 6 and 7).
805 This prevents *S. parvula* from experiencing a high-K induced N-starvation.

806 The depletion of N uptake in *A. thaliana* further descends into depletion of primary
807 metabolic pools rich in N (Fig 3D) with a concomitant transcriptional suppression observed in N
808 assimilation via the GS-GOGAT pathway (Fig 7) (O'Brien et al., 2016; Ji et al., 2019). This not
809 only creates a shortage of essential primary metabolic pools required for growth and
810 development, but also depletes essential antioxidant and osmolyte pools to defend against the
811 mounting oxidative and osmotic stresses (Fig 3, 7, 9). High K in the growth medium is known to
812 exert osmotic stress at a comparable level to Na and can also lead to oxidative damage
813 (Osakabe et al., 2013; Zheng et al., 2013). This creates an overall need to boost osmotic and
814 antioxidant defense systems to successfully survive high K^+ toxicity stress.
815 Accumulation of compatible osmolytes during osmotic stress reduces water loss from
816 tissues and helps to maintain turgor pressure which in turn would allow plants to regulate
817 water transport and photosynthesis (Apse and Blumwald, 2000). Synergistic transcriptional and
818 metabolic resource allocation to increase osmoprotectants during high K^+ stress is much more
819 pronounced in *S. parvula* than in *A. thaliana*. Among several osmolytes highlighted in our
820 results earlier, *S. parvula* roots and shoots notably accumulated significantly higher levels of
821 proline. Further, the precursors to proline, glutamine and glutamate, accumulated in *S. parvula*
822 roots (Fig 3 and 7). Stress tolerance upon increased accumulation of proline resulting from both
823 increased synthesis and reduced catabolism has been previously shown as a key adaptive
824 mechanism in *E. salsugineum* during salt stress, an extremophyte relative of *S. parvula* (Kant et
825 al., 2006). Proline plays an important role by serving as an osmolyte, and an antioxidant, and is
826 reported to facilitate increased photosynthesis during salt stress in many plants (Kishor et al.,
827 1995; Gong et al., 2005; Kumar et al., 2010; Ghanti et al., 2011; Hayat et al., 2012).
828 K and N together and independently regulate phosphorus (P) uptake into plants (Coskun
829 et al., 2017; Maeda et al., 2018; Cui et al., 2019). Additionally, high K^+ toxicity has been reported
830 to induce P-starvation (Ródenas et al., 2019). Therefore, K and N status of a plant serve as a key
831 determinant that controls the overall nutrient uptake processes including P uptake in plants
832 and availability of defense compounds required during salt stress. During high K-induced N-
833 starved conditions, *A. thaliana* experienced severe shortages of multiple key nutrients (Fig 2),
834 which *S. parvula* seemingly avoided by having independent regulatory capacity of K and N

835 uptake and remobilization (Fig 6, 7, and 9). Therefore, we propose that the ability to regulate
836 independent K^+ uptake is the first key deterministic step towards building resilience to high
837 external K^+.

838 **Efficient transcriptional resource allocation vs transcriptional mismanagement**

839 Pleiotropic K signaling beneficial under low K conditions lead to wasteful transcriptional
840 resources during high K^+ conditions in *A. thaliana* and leads to futile activation of multiple
841 hormone signaling pathways. K serves as a key signaling molecule for hormonal regulation
842 required for developmental processes, biotic stress signaling, and abiotic stress signaling (Zhang
843 et al., 2014; Hauser et al., 2017; Shabala, 2017; Hughes et al., 2020; Hetherington et al., 2021).
844 Plants constantly sense and adjust growth and development based on nutrient availability, and
845 in the context of K availability, all canonical mechanisms described for hormone-dependent
846 growth modifications that involve sensing K^+ are based on sensing external K^+ at low or growth
847 favorable conditions. When supplied with toxic levels of K^+ for most plants, we found that *A.*
848 *thaliana* was unable to adjust the K-dependent signaling to fit the extant specific stress
849 condition and allowed non- selective hormone signaling pathways to be transcriptionally
850 regulated (Fig 4). This would have led to transcriptional resource mismanagement especially
851 when biotic stress response pathways were activated concurrent to depleted N-sources and
852 when it was at a comparable level of proportional allocation assigned to abiotic stress
853 management (Fig 2, 3, 4B, 5, and S5). This level of non-selective transcriptional activity is
854 indicative of transcriptional mismanagement in *A. thaliana* seen at 24 HAT and it is not a
855 signature of deregulation or lack of regulation expected from dying plants as we observe a clear
856 decline in such non-selective pathway regulation by 72 HAT of exposure to high K^+ (Fig 4B).
857 Therefore, we propose that the capacity to avoid non-selective transcriptional mismanagement
858 is the second major deterministic step in surviving high K^+ stress. If unavoided, it can lead to
859 systemic damage via activation of ROS and autophagy pathways, as demonstrated by *A.*
860 *thaliana* with its increased ROS accumulation perhaps resulting from induction of biotic stress
861 responses or unmitigated oxidative stresses directly induced by high K^+ detrimental especially
862 at a nutrient starved environment created by high K^+ (Fig 4). ROS signals are known to induce
863 autophagy often associated with abiotic and biotic stress responses, and during nutrient

recycling, in addition to several plant developmental processes (Liu et al., 2005; Thompson et al., 2005; Lv et al., 2014; Pantha and Dassanayake, 2020). However, uncontrolled or misregulated initiation of autophagy signifies a failed stress response strategy (Floyd et al., 2015). In *A. thaliana* shoots, autophagy is the most enriched transcriptional pathway active at 24 and 72 HAT. The collective transcriptional signal enriched for pathways associated with lipid catabolism, protein degradation, DNA repair, cell death, and leaf senescence (Das and Roychoudhury, 2014) (Fig 4B) is further indicative of the maladaptive stress response strategies shown by *A. thaliana* contrasted against *S. parvula* which shows a more refined transcriptional response to survive high K^+ stress. The *S. parvula* transcriptome shows a pre-adapted state to high K^+ stress when examined together with co-expressed orthologs in *A. thaliana. S. parvula* mostly activates a limited yet focused response towards achieving stress tolerance while supporting overall growth and metabolism (Fig 5 and 8). Extremophyte transcriptomes and metabolomes including previous reports on *S. parvula* have shown similar stress-ready states constant stresses frequently associated with their native environments (Kant et al., 2006; Lugan et al., 2010; Oh et al., 2014; Lee et al., 2021; Wang et al., 2021).

In conclusion, upon exposure to high K^+, plants undergo physiological, metabolic, and transcriptional changes and a subset of those changes lead to stress adaptive traits while the other responses are indicative of failed cellular responses unable to meet the increasing systemic stress exerted by excess K^+ retention in tissues. The deterministic step whether a plant would be able to survive K-induced salt stress or descend into unmitigated stress responses was primarily set early on in the ability to regulate K uptake independent from other nutrient uptake pathways. This decoupled regulation of K sensing and stress signaling can be leveraged to design improved crops that are better able to dynamically adjust to a wide array of soils or irrigation water sources with different salt compositions.

Acknowledgements

We thank Dr. Guannan Wang, Kieu-Nga Tran, Chathura Wijesinghege, Dr. Aaron Smith, and Dr. John Larkin for providing feedback on the manuscript and facilitating helpful discussions; Prava Adhikari for additional assistance with phenotyping, and undergraduate students Saad

Chaudhari, Megan Guilbeau, and August Steinkamp for their assistance to grow plants. This work was supported by the US National Science Foundation awards MCB-1616827 and IOS-EDGE-1923589, US Department of Energy BER-DE-SC0020358, and the Next-Generation BioGreen21 Program of Republic of Korea (PJ01317301) awarded to MD and DHO. PP was supported by an Economic Development Assistantship award from Louisiana State University. We acknowledge the LSU High Performance Computing services for providing computational resources needed for data analyses.

Author Contributions

PP conducted experiments and performed data analyses. DL supervised and assisted with measuring CO_2 assimilation rates. DHO provided bioinformatics assistance. MD developed the experimental design and supervised the overall project. PP and MD interpreted results and wrote the article with input from all co-authors who revised and approved the final manuscript.

References

Ali A, Khan IU, Jan M, Khan HA, Hussain S, Nisar M, Chung WS, Yun D-J (2018) The High-Affinity Potassium Transporter EpHKT1;2 From the Extremophile Eutrema parvula Mediates Salt Tolerance. Front Plant Sci **9**: 1–11

Ali A, Raddatz N, Aman R, Kim S, Park HC, Jan M, Baek D, Khan IU, Oh D, Lee SY, et al (2016) A Single Amino-Acid Substitution in the Sodium Transporter HKT1 Associated with Plant Salt Tolerance. Plant Physiol **171**: 2112–2126

Andrews S (2010) FastQC: A quality control tool for high throughput sequence data. Babraham Bioinforma http://www.bioinformatics.babraham.ac.uk/projects/

Apse MP, Blumwald E (2000) Engineering salt tolerance in plants. Curr Opin Biotechnol **13**: 146–150

Aquea F, Federici F, Moscoso C, Vega A, Jullian P, Haseloff J, Arce-Johnson P (2012) A molecular framework for the inhibition of Arabidopsis root growth in response to boron toxicity. Plant, Cell Environ **35**: 719–734

Arienzo M, Christen EW, Quayle W, Kumar A (2009) A review of the fate of potassium in the soil-plant system after land application of wastewaters. J Hazard Mater **164**: 415–422

Armengaud P, Breitling R, Amtmann A (2004) The Potassium-Dependent Transcriptome of Arabidopsis Reveals a Prominent Role of Jasmonic Acid in Nutrient Signaling. Plant Physiol **136**: 2556–2576

Ashby WC, Beadle NCW (1957) Studies in Halophytes : III . Salinity Factors in the Growth of Australian Saltbushes Author (s): W . C . Ashby and N . C . W . Beadle Published by : Wiley on behalf of the Ecological Society of America Stable URL :

https://www.jstor.org/stable/1931695. Ecology **38**: 344–352

Ashley MK, Grant M, Grabov A (2006) Plant responses to potassium deficiencies: a role for potassium transport proteins. J Exp Bot **57**: 425–436

Bassil E, Zhang S, Gong H, Tajima H, Blumwald E (2019) Cation specificity of vacuolar NHX-type cation/H + Antiporters 1. Plant Physiol **179**: 616–629

Baxter IR, Ziegler G, Lahner B, Mickelbart M V, Foley R, Danku J, Armstrong P, Salt DE, Hoekenga OA (2014) Single-Kernel Ionomic Profiles Are Highly Heritable Indicators of Genetic and Environmental Influences on Elemental Accumulation in Maize Grain (Zea mays). PLoS One. doi: 10.1371/journal.pone.0087628

Chen CZ, Lv XF, Li JY, Yi HY, Gong JM (2012) Arabidopsis NRT1.5 is another essential component in the regulation of nitrate reallocation and stress tolerance. Plant Physiol **159**: 1582–1590

Conway JR, Lex A, Gehlenborg N (2017) UpSetR : an R package for the visualization of intersecting sets and their properties. **33**: 2938–2940

Coskun D, Britto DT, Kronzucker HJ (2017) The nitrogen–potassium intersection: membranes, metabolism, and mechanism. Plant Cell Environ **40**: 2029–2041

Cramer GR, Epstein E, Lauchli A (1990) Effects of sodium , potassium and calcium on salt-stressed barley . I . Growth analysis. 83–88

Cui Y, Li X, Yuan J, Wang F, Wang S (2019) Biochemical and Biophysical Research Communications Nitrate transporter NPF7 . 3 / NRT1 . 5 plays an essential role in regulating phosphate de fi ciency responses in Arabidopsis. Biochem Biophys Res Commun **508**: 314–319

Das K, Roychoudhury A (2014) Reactive oxygen species (ROS) and response of antioxidants as ROS-scavengers during environmental stress in plants. Front Environ Sci **2**: 1–13

Dassanayake M, Oh D-H, Haas JS, Hernandez A, Hong H, Ali S, Yun D-J, Bressan R a, Zhu J-K, Bohnert HJ, et al (2011) The genome of the extremophile crucifer Thellungiella parvula. Nat Genet **43**: 913–918

Daudi A, O'Brien JA (2012) Detection of Hydrogen Peroxide by DAB Staining in. Bio-protocol **2**: e263

Demidchik V, Straltsova D, Medvedev SS, Pozhvanov GA, Sokolik A (2014) Stress-induced electrolyte leakage : the role of K+ -permeable channels and involvement in programmed cell death and metabolic adjustment. J Exp Bot **65**: 1259–1270

Dietrich P, Moeder W, Yoshioka K (2020) Plant cyclic nucleotide-gated channels: New insights on their functions and regulation. Plant Physiol **184**: 27–38

Dijkshoorn W, Lathwell DJ, Wit CTDE (1968) Temporal changes in carboxylate content of ryegrass with stepwise change in nutrition. Plant Soil

Dreyer I, Gomez-Porras JL, Riedelsberger J (2017) The potassium battery: a mobile energy source for transport processes in plant vascular tissues. New Phytol **216**: 1049–1053

Duval JS, Carson JM, Holman PB, Darnley AG (2005) Terrestrial Radioactivity and Gamma-ray Exposure in the United States and Canada. US Geol Surv Open-File Rep 1413:

Eijk VM (1939) Analysis of the effect of NaCl on development, succulence and transpiration in Salicornia herbacea, as well as studies on the influence of salt uptake on root respiration in Aster Tripolium. Recl des Trav Bot néerlandais **36**: 559–657

Eshel A (1985) Response of Suaeda aegyptiaca to KCl, NaCl and Na2SO4 treatments. Physiol Plant **64**: 308–315

973 **Feng H, Fan X, Miller AJ, Xu G** (2020) Plant nitrogen uptake and assimilation: Regulation of
974 cellular pH homeostasis. J Exp Bot **71**: 4380–4392
975 **Ferreira T, Rasband W** (2012) ImageJ User Guide User Guide ImageJ.
976 **Fiehn O, Wohlgemuth G, Scholz M, Kind T, Lee DY, Lu Y, Moon S, Nikolau B** (2008) Quality
977 control for plant metabolomics: Reporting MSI-compliant studies. Plant J **53**: 691–704
978 **Floyd BE, Pu Y, Soto-Burgos J, Bassham DC** (2015) To Live or Die: Autophagy in Plants. In:
979 Gunawardena A., McCabe P. (eds) Plant Programmed Cell Death. Springer, Cham
980 **Gasch AP, Eisen MB** (2002) Exploring the conditional coregulation of yeast gene expression
981 through fuzzy k-means clustering. Genome Biol. doi: 10.1186/gb-2002-3-11-research0059
982 **Gaymard F, Pilot G, Lacombe B, Bouchez D, Bruneau D, Boucherez J, Michaux-Ferrière N,**
983 **Thibaud JB, Sentenac H** (1998) Identification and disruption of a plant shaker-like outward
984 channel involved in K+release into the xylem sap. Cell **94**: 647–655
985 **Ghanti SKK, Sujata KG, Kumar BMV, Karba NN** (2011) Heterologous expression of P5CS gene in
986 chickpea enhances salt tolerance without affecting yield. Biol Plant **55**: 634–640
987 **Gierth M, Mäser P, Schroeder JI** (2005) The potassium transporter AtHAK5 functions in K(+)
988 deprivation-induced high-affinity K(+) uptake and AKT1 K(+) channel contribution to K(+)
989 uptake kinetics in Arabidopsis roots. Plant Physiol **137**: 1105–14
990 **Gobert A, Isayenkov S, Voelker C, Czempinski K, Maathuis FJM** (2007) The two-pore channel
991 TPK1 gene encodes the vacuolar K ⁄. conductance and plays a role in K ⁄. homeostasis.
992 Proc Natl Acad Sci USA **104**: 10726–10731
993 **Gobert A, Park G, Amtmann A, Sanders D, Maathuis FJM** (2006) Arabidopsis thaliana Cyclic
994 Nucleotide Gated Channel 3 forms a non-selective ion transporter involved in germination
995 and cation transport. J Exp Bot **57**: 791–800
996 **Gong Q, Li P, Ma S, Indu Rupassara S, Bohnert HJ** (2005) Salinity stress adaptation competence
997 in the extremophile *Thellungiella halophila* in comparison with its relative *Arabidopsis*
998 *thaliana*. Plant J **44**: 826–839
999 **Gu Z, Gu L, Eils R, Schlesner M, Brors B** (2014) circlize implements and enhances circular
1000 visualization in R. Bioinformatics **30**: 2811–2812
1001 **Guo K, Babourina O, Christopher DA, Borsics T, Rengel Z** (2008) The cyclic nucleotide-gated
1002 channel, AtCNGC10, influences salt tolerance in Arabidopsis. Physiol Plant **134**: 499–507
1003 **Han M, Wu W, Wu WH, Wang Y** (2016) Potassium Transporter KUP7 Is Involved in K+
1004 Acquisition and Translocation in Arabidopsis Root under K+-Limited Conditions. Mol Plant
1005 **9**: 437–446
1006 **Hauser F, Li Z, Waadt R, Schroeder JI** (2017) SnapShot: Abscisic Acid Signaling. Cell **171**: 1708-
1007 1708.e0
1008 **Hayat S, Hayat Q, Alyemeni MN, Wani AS, Pichtel J, Ahmad A, Hayat S, Hayat Q, Alyemeni**
1009 **MN, Wani AS, et al** (2012) Role of proline under changing environments A review Role of
1010 proline under changing environments A review. doi: 10.4161/psb.21949
1011 **Hetherington FM, Kakkar M, Topping JF, Lindsey K** (2021) Gibberellin signaling mediates lateral
1012 root inhibition in response to K+ -deprivation. Plant Physiol **185**: 1198–1215
1013 **Hughes AM, Zwack PJ, Cobine PA, Rashotte AM** (2020) Cytokinin-regulated targets of Cytokinin
1014 Response Factor 6 are involved in potassium transport. Plant Direct 1–15
1015 **IPCC** (2019) Climate Change and Land: an IPCC special report on climate change, desertification,
1016 land degradation, sustainable land management, food security, and greenhouse gas fluxes

1017 in terrestrial ecosystems [P.R. Shukla, J. Skea, E. Calvo Buendia, V. Masson-De.
1018 **Ivashikina N, Dirk B, Ache P, Meyerho O, Felle HH, Hedrich R** (2001) K+ channel profile and
1019 electrical properties of Arabidopsis root hairs. FEBS Lett **508**: 463–469
1020 **Jabs T, Dietrich RA, Dangl JL** (1996) Initiation of runaway cell death in an Arabidopsis mutant by
1021 extracellular superoxide. Science (80-) **273**: 1853–1856
1022 **Ji Y, Li Q, Liu G, Selvaraj G, Zheng Z, Zou J, Wei Y** (2019) Roles of Cytosolic Glutamine
1023 Synthetases in Arabidopsis Development and Stress Responses. Plant Cell Physiol **60**: 657–
1024 671
1025 **Kanehisa M, Sato Y, Kawashima M, Furumichi M, Tanabe M** (2016) KEGG as a reference
1026 resource for gene and protein annotation. Nucleic Acids Res **44**: D457–D462
1027 **Kant S, Kant P, Raveh E, Barak S** (2006) Evidence that differential gene expression between the
1028 halophyte, Thellungiella halophila, and Arabidopsis thaliana is responsible for higher levels
1029 of the compatible osmolyte proline and tight control of Na+ uptake in T. halophila. Plant,
1030 Cell Environ **29**: 1220–1234
1031 **Kazachkova Y, Eshel G, Pantha P, Cheeseman JM, Dassanayake M, Barak S** (2018)
1032 Halophytism: What Have We Learnt From Arabidopsis Relative Model Systems? Plant
1033 Physiol **178**: 972–988
1034 **Kim MJ, Ruzicka D, Shin R, Schachtman DP** (2012) The Arabidopsis AP2 / ERF Transcription
1035 Factor RAP2 . 11 Modulates Plant Response to Low-Potassium Conditions. Mol Plant **5**:
1036 1042–1057
1037 **Kishor PBK, Hong Z, Miao C-H, Hu C-AA, Verma DPS** (1995) Overexpression of A1-Pyrroline-5-
1038 Carboxylate Synthetase Increases Proline Production and Confers Osmotolerance in
1039 Transgenic Plants '. Plant Physiol **108**: 1387–1394
1040 **Kolde R** (2012) pheatmap v.1.0.8. https://cran.r-project.org/package=pheatmap 1–7
1041 **Kumar V, Shriram V, Kishor PBK** (2010) Enhanced proline accumulation and salt stress
1042 tolerance of transgenic indica rice by over-expressing P5CSF129A gene. Plant Biotechnol
1043 Rep **4**: 37–48
1044 **Langmead B, Trapnell C, Pop M, Salzberg SL** (2009) Ultrafast and memory-efficient alignment
1045 of short DNA sequences to the human genome. Genome Biol **10**: R25
1046 **Lee G, Ahmadi H, Quintana J, Syllwasschy L, Preite V, Anderson JE, Genetics M, Information C,**
1047 **Footnotes A** (2021) Constitutively enhanced genome integrity maintenance and direct
1048 stress mitigation characterize transcriptome of extreme stress-adapted Arabidopsis halleri.
1049 bioRxiv
1050 **Leigh R, Wyn Jones RG** (1984) A hypothesis relating critical potassium concentrations for
1051 growth to the distribution and function of this ion in the plant cell. New Phytol. 97. 1–13
1052 **Lequeux H, Hermans C, Lutts S, Verbruggen N** (2010) Response to copper excess in Arabidopsis
1053 thaliana: Impact on the root system architecture, hormone distribution, lignin
1054 accumulation and mineral profile. Plant Physiol Biochem **48**: 673–682
1055 **Li H, Yu M, Du XQ, Wang ZF, Wu WH, Quintero FJ, Jin XH, Li HD, Wang Y** (2017) NRT1.5/NPF7.3
1056 functions as a proton-coupled H+/K+ antiporter for K+ loading into the xylem in
1057 arabidopsis. Plant Cell **29**: 2016–2026
1058 **Li JY, Fu YL, Pike SM, Bao J, Tian W, Zhang Y, Chen CZ, Zhang Y, Li HM, Huang J, et al** (2010)
1059 The Arabidopsis nitrate transporter NRT1.8 functions in nitrate removal from the xylem
1060 sap and mediates cadmium tolerance. Plant Cell **22**: 1633–1646

1061 **Liu Y, Schiff M, Czymmek K, Tallóczy Z, Levine B, Dinesh-Kumar SP** (2005) Autophagy regulates
1062 programmed cell death during the plant innate immune response. Cell **121**: 567–577
1063 **Love MI, Huber W, Anders S** (2014) Moderated estimation of fold change and dispersion for
1064 RNA-seq data with DESeq2. Genome Biol **15**: 550
1065 **Lugan R, Niogret MF, Leport L, Guégan JP, Larher FR, Savouré A, Kopka J, Bouchereau A** (2010)
1066 Metabolome and water homeostasis analysis of Thellungiella salsuginea suggests that
1067 dehydration tolerance is a key response to osmotic stress in this halophyte. Plant J **64**:
1068 215–229
1069 **Lv X, Pu X, Qin G, Zhu T, Lin H** (2014) The roles of autophagy in development and stress
1070 responses in Arabidopsis thaliana. Apoptosis **19**: 905–921
1071 **Maathuis FJ** (2009) Physiological functions of mineral macronutrients. Curr Opin Plant Biol **12**:
1072 250–258
1073 **Maeda Y, Konishi M, Kiba T, Sakuraba Y, Sawaki N, Kurai T, Ueda Y, Sakakibara H, Yanagisawa**
1074 **S** (2018) A NIGT1-centred transcriptional cascade regulates nitrate signalling and
1075 incorporates phosphorus starvation signals in Arabidopsis. Nat Commun. doi:
1076 10.1038/s41467-018-03832-6
1077 **Maere S, Heymans K, Kuiper M** (2005) BiNGO: A Cytoscape plugin to assess overrepresentation
1078 of Gene Ontology categories in Biological Networks. Bioinformatics **21**: 3448–3449
1079 **Matoh T, Watanabe J, Takahashi E** (1986) Effects of Sodium and Potassium Salts on the Growth
1080 of a Halophyte. Soil Sci Plant Nutr **32**: 451–459
1081 **Murashige T, Skoog F** (1962) A Revised Medium for Rapid Growth and Bio Assays with Tobacco
1082 Tissue Cultures. Physiol Plant **15**: 473–497
1083 **Neuhauser B, Dynowski M, Mayer M, Ludewig U** (2007) Regulation of NH 4 1 Transport by
1084 Essential Cross Talk between AMT Monomers through the. Plant Physiol **143**: 1651–1659
1085 **Nilhan TG, Emre YA, Osman K** (2008) Soil Determinants for distribution of Halocnemum
1086 strobilaceum Bieb. (Chenopodiaceae)Around Lake Tuz, Turkey. Pakistan J Biol Sci **11**: 565–
1087 570
1088 **Nishizawa A, Yabuta Y, Shigeoka S** (2008) Galactinol and Raffinose Constitute a Novel Function
1089 to Protect Plants from Oxidative Damage. Plant Physiol **147**: 1251–1263
1090 **O'Brien JAA, Vega A, Bouguyon E, Krouk G, Gojon A, Coruzzi G, Gutiérrez RAA** (2016) Nitrate
1091 Transport, Sensing, and Responses in Plants. Mol Plant **9**: 837–856
1092 **Oh D-H, Dassanayake M** (2019) Landscape of gene transposition-duplication within the
1093 Brassicaceae family. DNA Res **26**: 21–36
1094 **Oh D-H, Hong H, Lee SY, Yun D-J, Bohnert HJ, Dassanayake M** (2014) Genome structures and
1095 transcriptomes signify niche adaptation for the multi-ion tolerant extremophyte
1096 *Schrenkiella parvula*. Plant Physiol **164**: 2123–2138
1097 **Oh D-H, Leidi E, Zhang Q, Hwang S-M, Li Y, Quintero FJ, Jiang X, D'Urzo MP, Lee SY, Zhao Y, et**
1098 **al** (2009) Loss of halophytism by interference with SOS1 expression. Plant Physiol **151**:
1099 210–222
1100 **Osakabe Y, Arinaga N, Umezawa T, Katsura S, Nagamachi K, Tanaka H, Ohiraki H, Yamada K,**
1101 **Seo S-U, Abo M, et al** (2013) Osmotic Stress Responses and Plant Growth Controlled by
1102 Potassium Transporters in Arabidopsis. Plant Cell **25**: 609–624
1103 **Pantha P, Chalivendra S, Oh DH, Elderd BD, Dassanayake M** (2021) A tale of two transcriptomic
1104 responses in agricultural pests via host defenses and viral replication. Int J Mol Sci **22**: 1–27

Pantha P, Dassanayake M (2020) Living with Salt. Innov **1**: 100050

Ragel P, Ródenas R, García-martín E, Andrés Z, Villalta I, Nieves-cordones M, Rivero RM, Martínez V, Pardo JM, Quintero FJ, et al (2015) The CBL-Interacting Protein Kinase CIPK23 Regulates HAK5-Mediated High-Af fi nity K + Uptake in Arabidopsis Roots 1 [OPEN]. Plant Physiol **169**: 2863–2873

Ramos J, López MJ, Benlloch M (2004) Effect of NaCl and KCl salts on the growth and solute accumulation of the halophyte Atriplex nummularia. Plant Soil **259**: 163–168

Richter JA, Behr JH, Erban A, Kopka J, Zörb C (2019) Ion-dependent metabolic responses of Vicia faba L. to salt stress. Plant Cell Environ **42**: 295–309

Ródenas R, Martinez V, Nieves-cordones M, Rubio F (2019) High External K + Concentrations Impair Pi Nutrition , Induce the Phosphate Starvation Response , and Reduce Arsenic Toxicity in Arabidopsis Plants. Int J Mol Sci **20**: 1–18

Shabala S (2017) Signalling by potassium: Another second messenger to add to the list? J Exp Bot **68**: 4003–4007

Shabala S, Cuin TA (2008) Potassium transport and plant salt tolerance. Physiol Plant **133**: 651–669

Shi H, Ishitani M, Kim C, Zhu J-K (2000) The Arabidopsis thaliana salt tolerance gene SOS1 encodes a putative Na+/H+ antiporter. Proc Natl Acad Sci USA **97**: 6896–6901

Srivastava AK, Penna S, Nguyen D Van, Tran LP (2014) Multifaceted roles of aquaporins as molecular conduits in plant responses to abiotic stresses. Crit Rev Biotechnol **8551**: 1–10

Straub T, Ludewig U, Neuhäuser B (2017) The Kinase CIPK23 Inhibits Ammonium Transport in Arabidopsis thaliana. Plant Cell **29**: 409–422

Szyroki A, Ivashikina N, Dietrich P, Roelfsema MRG, Ache P, Reintanz B, Deeken R, Godde M, Felle H, Steinmeyer R, et al (2001) KAT1 is not essential for stomatal opening. Proc Natl Acad Sci U S A **98**: 2917–2921

Taji T, Ohsumi C, Iuchi S, Seki M, Kasuga M, Kobayashi M, Yamaguchiâ€Shinozaki K, Shinozaki K (2002) Important roles of drought- and cold-inducible genes for galactinol synthase in stress tolerance in Arabidopsis thaliana. Plant J **29**: 417–426

Takahashi F, Shinozaki K (2019) Long-distance signaling in plant stress response. Curr Opin Plant Biol **47**: 106–111

Tegeder M, Masclaux-Daubresse C (2018) Source and sink mechanisms of nitrogen transport and use. New Phytol **217**: 35–53

Thompson AR, Doelling JH, Suttangkakul A, Vierstra RD (2005) Autophagic Nutrient Recycling in Arabidopsis Directed by the ATG8 and ATG12 Conjugation Pathways 1. Plant Physiol **138**: 2097–2110

Uozumi N, Kim EJ, Rubio F, Yamaguchi T, Muto S, Tsuboi a, Bakker EP, Nakamura T, Schroeder JI (2000) The Arabidopsis HKT1 gene homolog mediates inward Na(+) currents in xenopus laevis oocytes and Na(+) uptake in Saccharomyces cerevisiae. Plant Physiol **122**: 1249–1259

Voelker C, Schmidt D, Mueller-roeber B, Czempinski K (2006) Members of the Arabidopsis AtTPK / KCO family form homomeric vacuolar channels in planta. Plant J **48**: 296–306

Wang B, Lüttge U, Ratajczak R (2001) Effects of salt treatment and osmotic stress on V-ATPase and V-PPase in leaves of the halophyte Suaeda salsa. J Exp Bot **52**: 2355–2365

Wang G, DiTusa SF, Oh DH, Herrmann AD, Mendoza-Cozatl DG, O'Neill MA, Smith AP,

1149 **Dassanayake M** (2021) Cross species multi-omics reveals cell wall sequestration and
1150 elevated global transcription as mechanisms of boron tolerance in plants. New Phytol. doi:
1151 10.1101/2020.10.01.321760
1152 **Wang G, Oh D, Dassanayake M** (2020) GOMCL: a toolkit to cluster, evaluate, and extract non-
1153 redundant associations of Gene Ontology-based functions. BMC Bioinformatics **21**: 1–9
1154 **Wang X-P, Li-MeiChen, Liu W-X, Shen L-K, Wang F-L, Zhou Y, Zhang Z, Wu W-H, Wang Y** (2016)
1155 AtKC1 and CIPK23 Synergistically Modulate AKT1-Mediated Low-Potassium Stress. Plant
1156 Physiol **170**: 2264–2277
1157 **Wang Y, Wu W-H** (2013) Potassium Transport and Signaling in Higher Plants. Annu Rev Plant
1158 Biol **64**: 451–476
1159 **Warren JK** (2016) Potash Resources: Occurrences and Controls. Evaporites A Geol Compend.
1160 doi: 10.1007/978-3-319-13512-0_11
1161 **Xu J, Li HD, Chen LQ, Wang Y, Liu LL, He L, Wu WH** (2006) A Protein Kinase, Interacting with
1162 Two Calcineurin B-like Proteins, Regulates K+ Transporter AKT1 in Arabidopsis. Cell **125**:
1163 1347–1360
1164 **Yoshitake Y, Nakamura S, Shinozaki D, Izumi M** (2021) RCB-mediated chlorophagy caused by
1165 oversupply of nitrogen suppresses phosphate-starvation stress in plants. Plant Physiol **185**:
1166 318–330
1167 **Yuan L, Loqué D, Kojima S, Rauch S, Ishiyama K, Inoue E, Takahashi H, Von Wirén N** (2007) The
1168 organization of high-affinity ammonium uptake in Arabidopsis roots depends on the
1169 spatial arrangement and biochemical properties of AMT1-type transporters. Plant Cell **19**:
1170 2636–2652
1171 **Yuen CCY, Christopher DA** (2013) The group IV-A cyclic nucleotide-gated channels, CNGC19 and
1172 CNGC20, localize to the vacuole membrane in Arabidopsis thaliana. AoB Plants **5**: 1–14
1173 **Zhang G Bin, Yi HY, Gong JM** (2014) The Arabidopsis Ethylene/Jasmonic acid-NRT signaling
1174 module coordinates nitrate reallocation and the trade-off between growth and
1175 environmental adaptation. Plant Cell **26**: 3984–3998
1176 **Zhao C, Zhang H, Song C, Zhu J-K, Shabala S** (2020) Mechanisms of Plant Responses and
1177 Adaptation to Soil Salinity. Innov **1**: 100017
1178 **Zhao S, Zhang M, Wang Y** (2016) Phosphorylation of ARF2 Relieves Its Repression of
1179 Transcription of the K + Transporter Gene HAK5 in Response to Low Potassium Stress.
1180 Plant Cell **28**: 3005–3019
1181 **Zheng S, Pan T, Fan L, Qiu Q** (2013) A Novel AtKEA Gene Family , Homolog of Bacterial K+/ H+
1182 Antiporters , Plays Potential Roles in K + Homeostasis and Osmotic Adjustment in
1183 Arabidopsis. PLoS One **8**: e81463
1184 **Ziegler G, Terauchi A, Becker A, Armstrong P, Hudson K, Baxter I** (2013) Ionomic Screening of
1185 Field-Grown Soybean Identifies Mutants with Altered Seed Elemental Composition. Plant
1186 Genome **6**: 0
1187 **Zioni A BEN, Vaadia Y, Lips SH** (1971) Nitrate Uptake by Roots as Regulated by Nitrate
1188 Reduction Products of the Shoot. Physiol Plant **24**: 288–290

1189 **Figures**

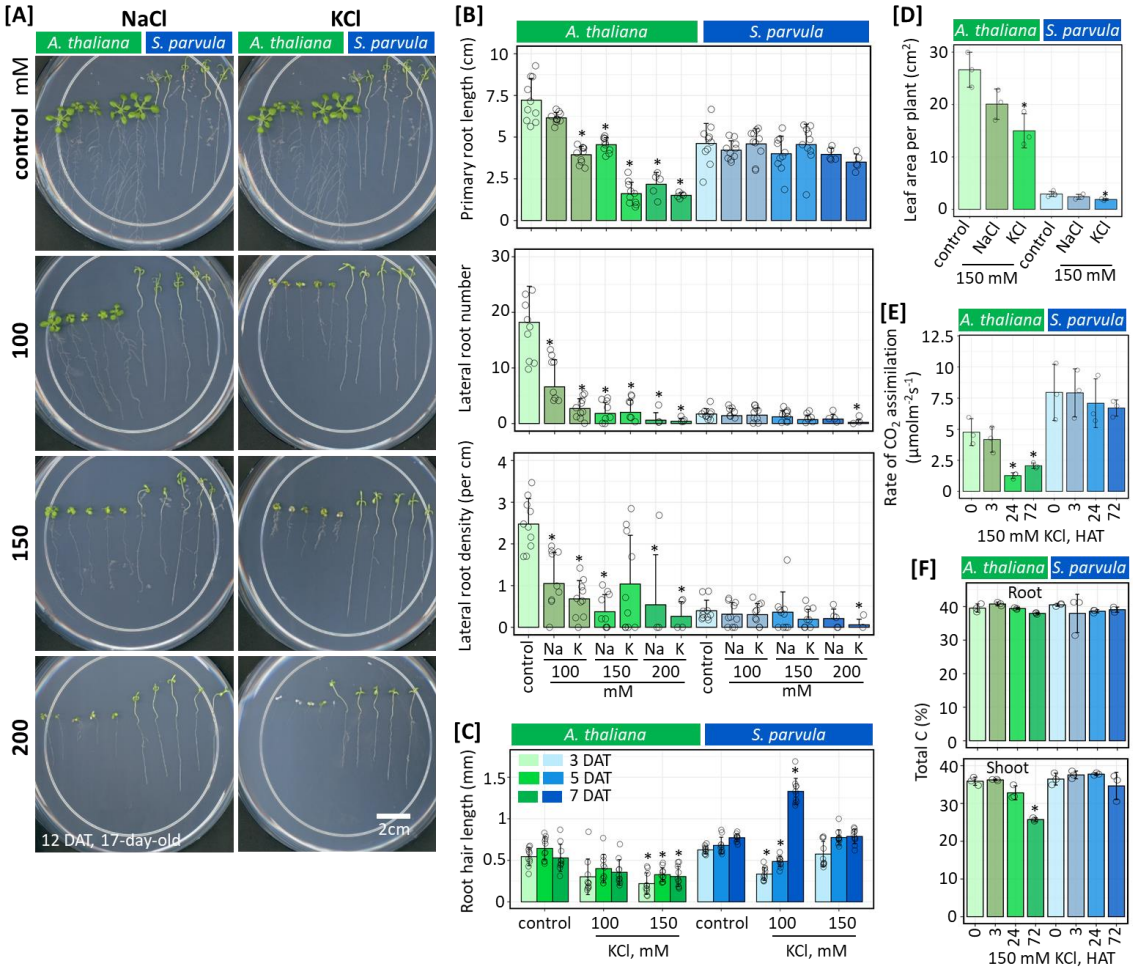

Figure 1. KCl is more toxic than NaCl at the same osmotic strength. [A] Seedlings of *Arabidopsis thaliana* (on the left for each plate) and *Schrenkiella parvula* (on the right for each plate) on 1/4 MS media supplemented with 0 to 200 mM NaCl and KCl. **[B]** Primary root length, lateral root number, and lateral root density measured on 17-day-old seedlings grown under conditions used in [A] based on a 12-day treatment of NaCl or KCl. **[C]** Root hair length measured under the same growth conditions used in [A] for variable KCl treatments and monitored for a week. **[D]** Leaf area measured for 5- and 6-week-old hydroponically grown *A. thaliana* and *S. parvula* treated with increasing levels of NaCl and KCl for 1- and 3-weeks respectively. **[E]** Photosynthesis measured as the rate of CO_2 assimilation of the entire shoot/rosette in 25-day-old hydroponically grown plants and monitored up to 72 HAT. **[F]** Total carbon as a % weight based on total dry mass for root and shoot tissue under conditions used in [E]. Minimum 5 plants per condition used in B and C and a minimum of 3 plants per condition used for D and E. Asterisks indicate significant changes between the treated samples to its respective control samples (t-test with $p < 0.05$). Data are presented as mean of at least 3 independent biological replicates ± SD. DAT-Days after treatment, HAT- Hours after treatment.

1190

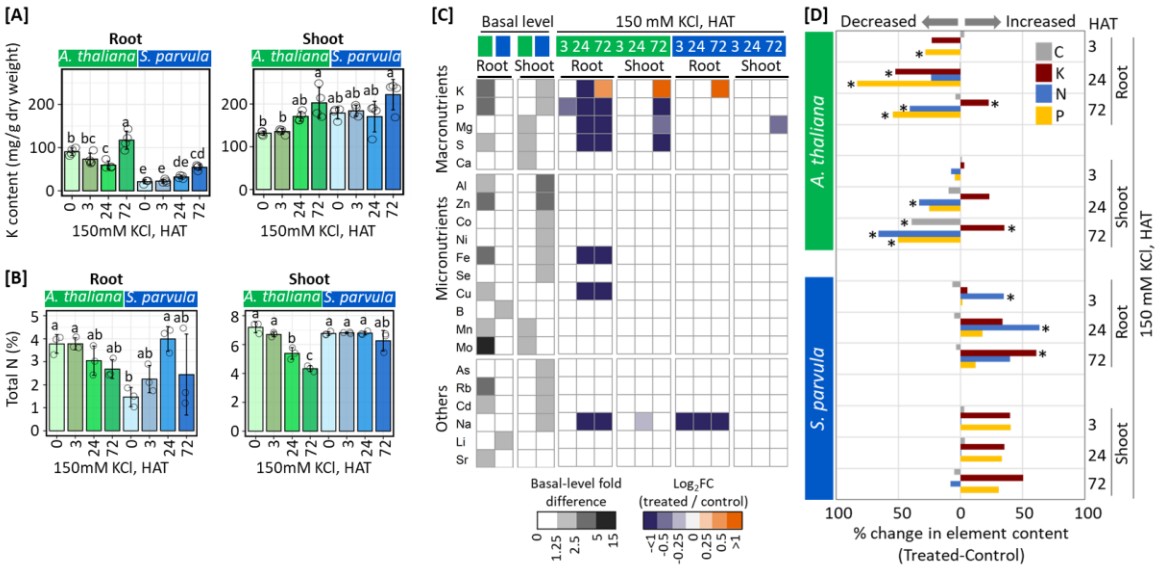

Figure 2. Excess K accumulation caused severe nutrient imbalance in *A. thaliana* compared to *S. parvula*. **[A]** K accumulated differently between *A. thaliana* and *S. parvula*. *A. thaliana* promoted shoot retention while *S. parvula* promoted root retention of K. **[B]** Increased accumulation of K resulted in N depletion in *A. thaliana* compared to *S. parvula*. **[C]** Differential accumulation of K caused imbalances of multiple nutrients in *A. thaliana* roots even in early time points and caused hardly any noticeable differences in *S. parvula*. **[D]** Percent change in CNPK elemental content in root and shoot of *A. thaliana* and *S. parvula* under high [K^+]. *A. thaliana* fails to maintain major macronutrient levels preventing depletion of those pools contrasted to *S. parvula*. Data are represented as mean of at least 4 (for A and C) and 3 (for B) independent replicates with ± SD given using ≥ 5-8 hydroponically grown plants per replicate. Elemental compositions were quantified using ICP-MS and total N was obtained using an elemental combustion system. The total elemental composition is reported after normalization for dry weight. All quantitative measurements were evaluated by one-way ANOVA followed by Tukey's post-hoc test, *p-value* <0.05 and same letters in the bar graph does not differ statistically significantly and asterisks indicate significant changes between the treated samples to its respective control samples. HAT- Hours after treatment.

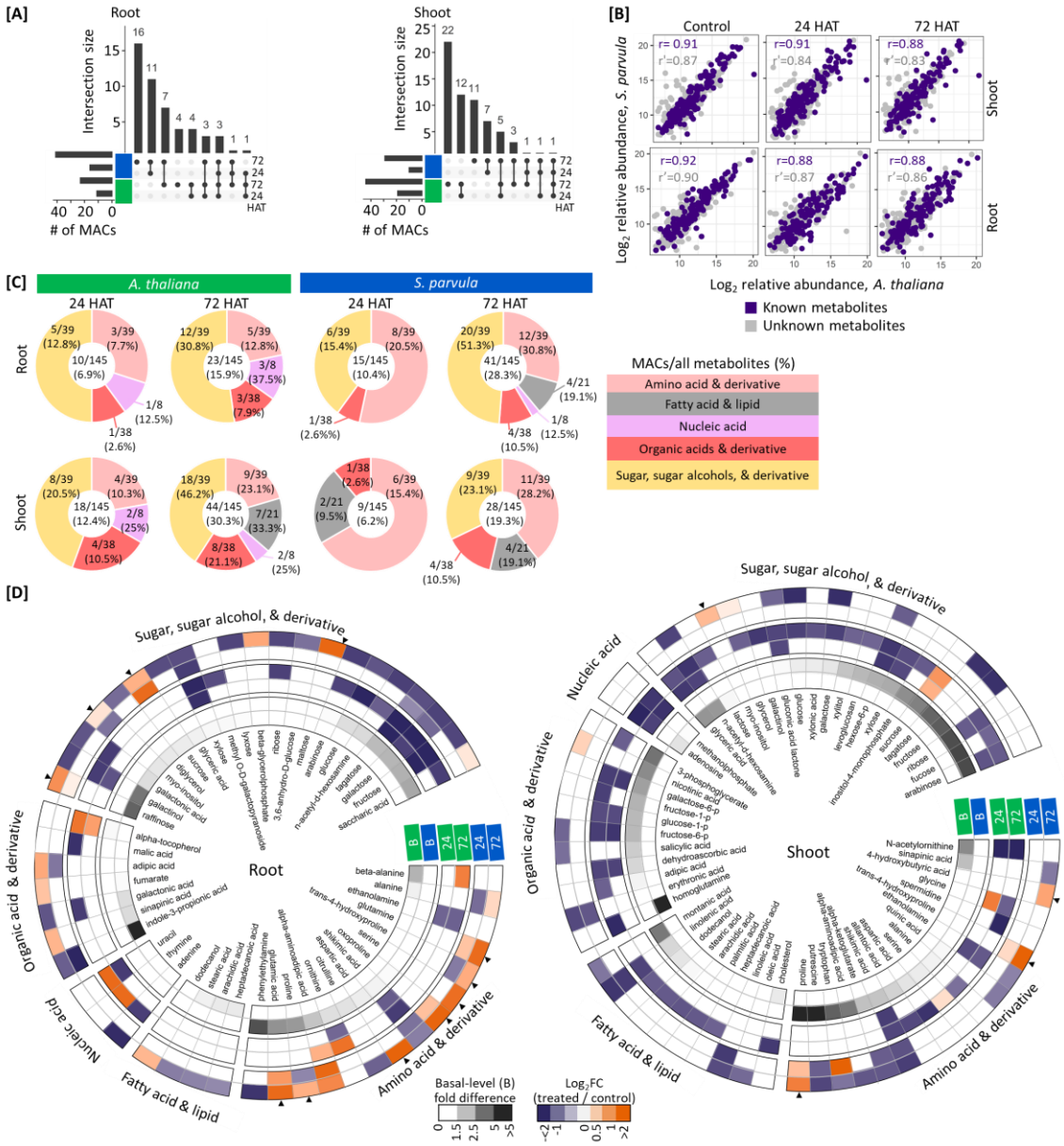

Figure 3. *S. parvula* root metabolome is more responsive than *A. thaliana* and induces specific antioxidants and osmoprotectants to adapt to high K^+ stress in both roots and shoots. **[A]** Metabolites that significantly changed in abundance at 24 and 72 hours after treatment (HAT). **[B]** *A. thaliana* and *S. parvula* metabolome profiles are highly corelated with each other upon high K^+ in both roots and shoots. Pearson correlation coefficient is calculated for 145 known metabolites (r) and all metabolites including the unannotated metabolites (r'). **[C]** Overview of the temporal changes in primary metabolic pools based on known metabolite annotations. Metabolites that significantly changed in abundance at respective time points are shown followed by a "/" and the total number of metabolites counted in that category. **[D]** Individual metabolites in each functional group mapped to represent their abundance starting at basal level (inner circles) to 24 and 72 h of exposure to high K shown in concentric outer rings. Metabolites mostly highlighted in Results and Discussion are marked with arrow heads in the outer circle in both plots. Significance test for metabolite abundance was performed with one-way ANOVA followed by Tukey's post-hoc test, *p-value* <0.05. Data are represented as mean of at least 3 independent replicates ± SD given using ≥ 5 hydroponically grown plants per replicate.

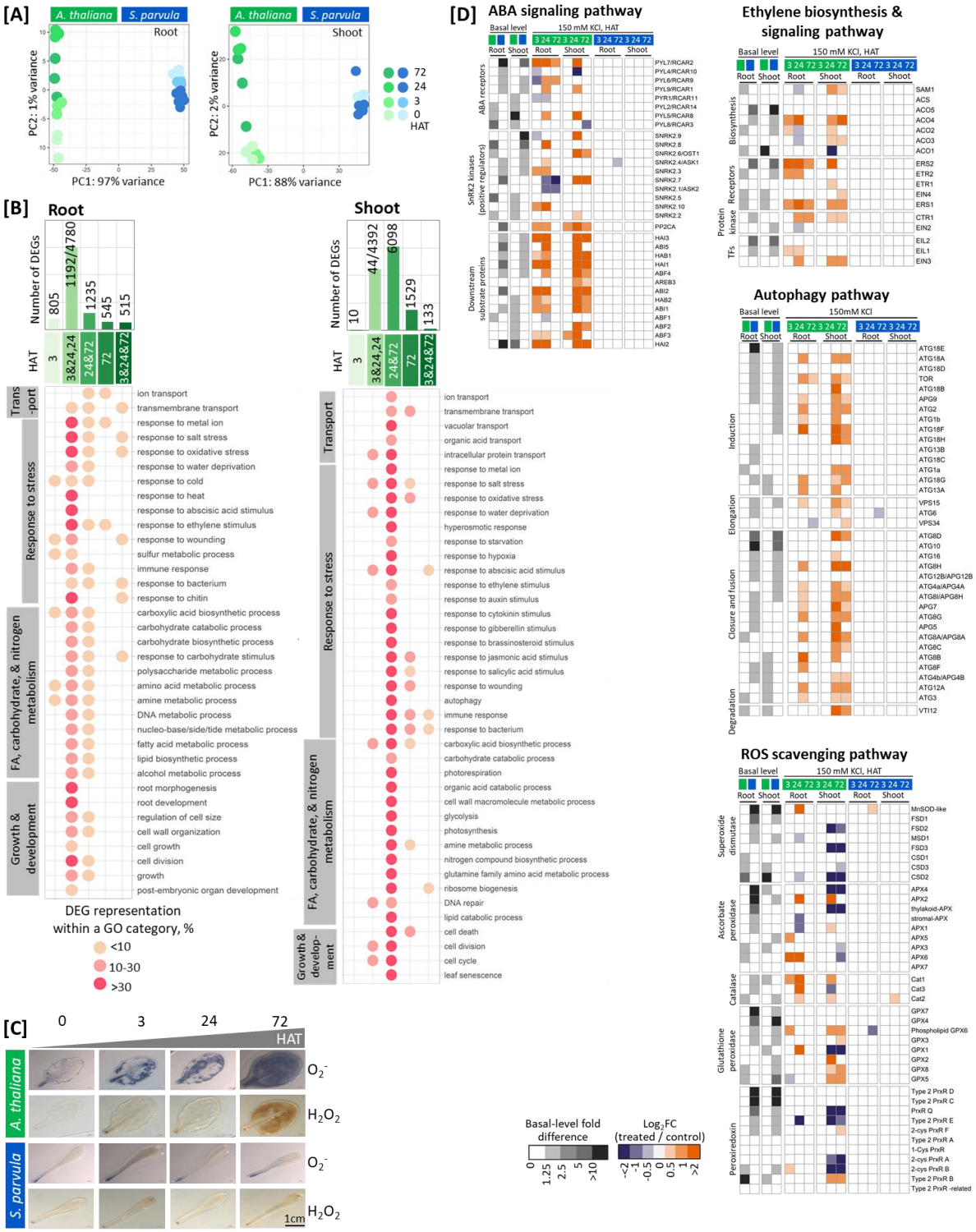
[A]
A. thaliana
S. parvula
Root
Shoot
PC2: 1% variance
PC1: 97% variance
PC2: 2% variance
PC1: 88% variance
72
24
3
0
HAT
[B]
Root
Shoot
Number of DEGs
805
1192/4780
1235
545
515
10
44/4392
6098
1529
133
HAT
3
3&24,24
24&72
72
3&24&72
Trans-port
Response to stress
FA, carbohydrate, & nitrogen metabolism
Growth & development
Transport
Growth & develop-ment
ion transport
transmembrane transport
response to metal ion
response to salt stress
response to oxidative stress
response to water deprivation
response to cold
response to heat
response to abscisic acid stimulus
response to ethylene stimulus
response to wounding
sulfur metabolic process
immune response
response to bacterium
response to chitin
carboxylic acid biosynthetic process
carbohydrate catabolic process
carbohydrate biosynthetic process
response to carbohydrate stimulus
polysaccharide metabolic process
amino acid metabolic process
amine metabolic process
DNA metabolic process
nucleo-base/side/tide metabolic process
fatty acid metabolic process
lipid biosynthetic process
alcohol metabolic process
root morphogenesis
root development
regulation of cell size
cell wall organization
cell growth
cell division
growth
post-embryonic organ development
vacuolar transport
organic acid transport
intracellular protein transport
hyperosmotic response
response to starvation
response to hypoxia
response to auxin stimulus
response to cytokinin stimulus
response to gibberellin stimulus
response to brassinosteroid stimulus
response to jasmonic acid stimulus
response to salicylic acid stimulus
autophagy
photorespiration
organic acid catabolic process
cell wall macromolecule metabolic process
glycolysis
photosynthesis
nitrogen compound biosynthetic process
glutamine family amino acid metabolic process
ribosome biogenesis
DNA repair
lipid catabolic process
cell death
cell cycle
leaf senescence
DEG representation within a GO category, %
<10
10-30
>30
[C]
0
3
24
72
HAT
A. thaliana
S. parvula
O_2^-
H_2O_2
1cm
[D]
ABA signaling pathway
Basal level
150 mM KCl, HAT
Root
Shoot
ABA receptors
SnRK2 kinases (positive regulators)
Downstream substrate proteins
PYL7/RCAR2
PYL4/RCAR10
PYL6/RCAR9
PYL9/RCAR1
PYR1/RCAR11
PYL2/RCAR14
PYL5/RCAR8
PYL8/RCAR3
SNRK2.9
SNRK2.8
SNRK2.6/OST1
SNRK2.4/ASK1
SNRK2.3
SNRK2.7
SNRK2.1/ASK2
SNRK2.5
SNRK2.10
SNRK2.2
PP2CA
HAI3
ABI5
HAB1
HAI1
ABF4
AREB3
ABI2
HAB2
ABI1
ABF1
ABF2
ABF3
HAI2
Ethylene biosynthesis & signaling pathway
Biosynthesis
Receptors
Protein kinase
TFs
SAM1
ACS
ACO5
ACO4
ACO2
ACO3
ACO1
ERS2
ETR2
ETR1
EIN4
ERS1
CTR1
EIN2
EIL2
EIL1
EIN3
Autophagy pathway
150mM KCl
Induction
Elongation
Closure and fusion
Degradation
ATG18E
ATG18A
ATG18D
TOR
ATG18B
APG9
ATG2
ATG1b
ATG18F
ATG18H
ATG13B
ATG18C
ATG1a
ATG18G
ATG13A
VPS15
ATG6
VPS34
ATG8D
ATG10
ATG16
ATG8H
ATG12B/APG12B
ATG4a/APG4A
ATG8I/APG8H
APG7
ATG8G
APG5
ATG8A/APG8A
ATG8C
ATG8B
ATG8F
ATG4b/APG4B
ATG12A
ATG3
VTI12
ROS scavenging pathway
Superoxide dismutase
Ascorbate peroxidase
Catalase
Glutathione peroxidase
Peroxiredoxin
MnSOD-like
FSD1
FSD2
MSD1
FSD3
CSD1
CSD3
CSD2
APX4
APX2
thylakoid-APX
stromal-APX
APX1
APX5
APX3
APX6
APX7
Cat1
Cat3
Cat2
GPX7
GPX4
Phospholipid GPX6
GPX3
GPX1
GPX2
GPX8
GPX5
Type 2 PrxR D
Type 2 PrxR C
PrxR Q
Type 2 PrxR E
2-cys PrxR F
Type 2 PrxR A
1-Cys PrxR
2-cys PrxR A
2-cys PrxR B
Type 2 PrxR B
Type 2 PrxR -related
Basal-level fold difference
0
1.25
2.5
5
>10
Log2FC (treated / control)
-<2
-1
-0.5
0
0.5
1
>2

1200

Figure 4. *A. thaliana* shows non-selective transcriptional modifications during excess K^+ stress than *S. parvula*. [A] Principal component analysis (PCA) of ortholog expression between *A. thaliana* and *S. parvula* root and shoot transcriptomes at 0, 3, 24, and 72 hours after treatment (HAT). **[B]** Enriched functional processes based on GO annotations associated with differently expressed genes (DEGs) in *A. thaliana*. The temporal sequence of enriched functions is given as 3 h specific, 3 and 24 h together with 24 h specific, and 72 h, 72 h specific, and present at all-time points from 3-24-72 h. Only functional processes that were detected at least in two time points are shown and the processes are sorted based on their functional hierarchy when applicable. **[C]** *A. thaliana* accumulated higher levels of hydrogen peroxide (H_2O_2) and superoxide ions (O_2^-) in leaves under excess K^+ stress compared to *S. parvula*. Hydroponically grown plants were used treated similar to the plants used for the RNA-Seq study and stained with DAB and NBT. **[D]** Transcriptional profiles of selected pathways that serve as indicators of transcriptional mismanagement in *A. thaliana* during excess K^+ stress compared to *S. parvula*. DEGs were called using DESeq2 with a p-adj value based on Benjamini-Hochberg correction for multiple testing set to <0.01.

1201
1202
1203
1204
1205
1206
1207
1208
1209
1210
1211
1212
1213
1214
1215
1216
1217

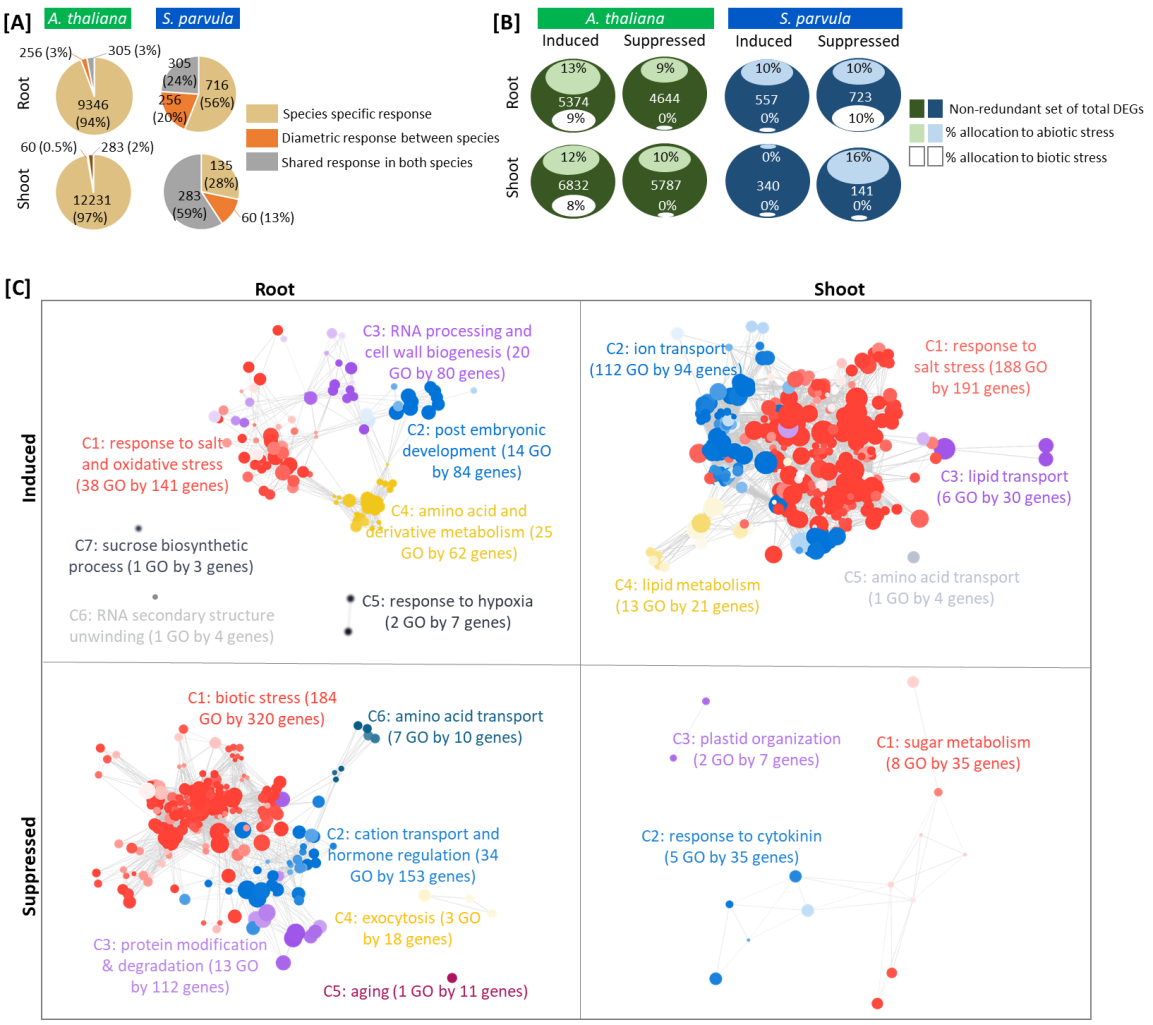

Figure 5. *S. parvula* shows a confined transcriptomic response geared toward concurrent induction of abiotic stress responses and enhanced transcriptional allocation to C and N metabolism. [A] The overall expression specificity and response direction of orthologs in *A. thaliana* and *S. parvula.* Selected orthologs are differentially expressed genes (DEGs) at least in one time point compared to the respective control condition and then counted as a non-redundant set when all 3, 24, and 72 HAT samples were considered for total counts. **[B]** The proportion contributing to abiotic and biotic stress stimuli within non-redundant DEGs. The effort to suppress biotic stress responses in *S. parvula* roots (10%) was similar to the proportional induction for biotic stress responses in *A. thaliana* (9%). **[C]** The functionally enriched processes represented by DEGs in *S. parvula* that responded to high K^+. A non-redundant set from all time points (3, 24, and 72 HAT) are given. A node in each cluster represents a gene ontology (GO) term; size of a node represents the number of genes included in that GO term; the clusters that represent similar functions share the same color and are given a representative cluster name and ID; and the edges between nodes show the DEGs that are shared between functions. All clusters included in the network have adj p-values <0.05 with false discovery rate correction applied. More significant values are represented by darker node colors. The functional enrichment network was created using GOMCL. DEGs were called using DESeq2 with a p-adj value based on Benjamini-Hochberg correction for multiple testing set to <0.01.

1218

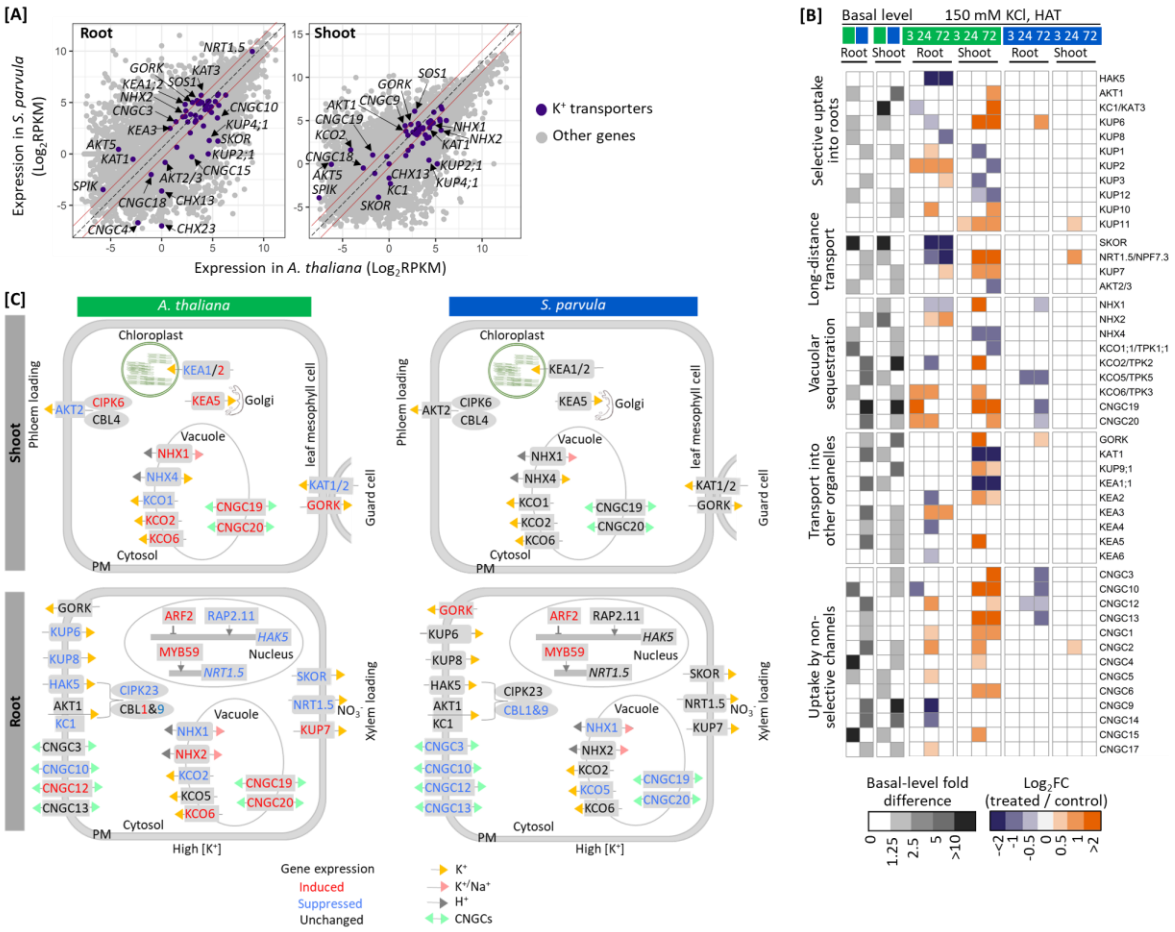

Figure 6. Differential expression of K⁺ transporters in *A. thaliana* and *S. parvula*. [A] Basal level expression comparison of orthologs between *A. thaliana* and *S. parvula* in roots and shoots. The dash-gray diagonal line marks identical expression in both species and solid red lines represent a 2-fold change in one species compared to the other species. Transporters/channels with >2-fold change basal differences between the species are labeled. **[B]** The temporal expression of functionally established K^+ transporters and channels in *A. thaliana* and their *S. parvula* orthologs upon high K^+ treatment. **[C]** Key K^+ transporters and channels differently regulated between roots and shoots in *A. thaliana* and *S. parvula*. DEGs at each time point were called using DESeq2 compared to 0 h with a p-adj value based on Benjamini-Hochberg correction for multiple testing set to <0.01.

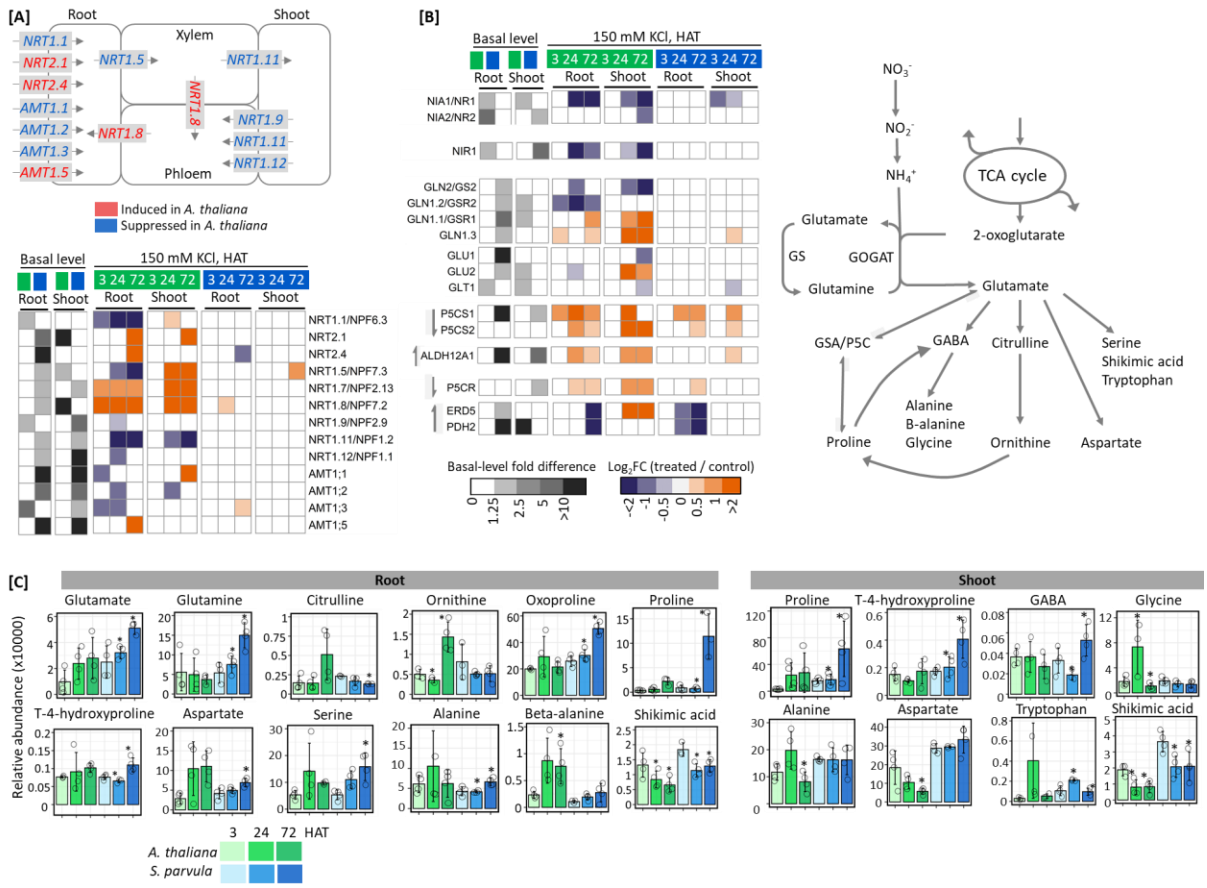

Figure 7. Excess K⁺ induced nitrogen starvation and suppressed associated N-assimilation pathways in *A. thaliana* compared to *S. parvula*. **[A]** Nitrogen uptake and distribution was severely affected in *A. thaliana* upon high K^+. The expression changes associated with major nitrogen transporters in *A. thaliana* that regulate root uptake and long-distance transport of N are summarized. **[B]** Coordinated transcriptional regulation showing high K^+-induced suppression of nitrogen assimilation and efforts to accumulate glutamate-derived osmoprotectants. The arrows in front of heatmap blocks indicate the direction of the reaction. **[C]** The primary metabolite pools derived from glutamate in roots and shoots. DEGs at each time point were called using DESeq2 compared to 0 h with a p-adj value based on Benjamini-Hochberg correction for multiple testing set to <0.01. Significance test for metabolite abundances was performed with one-way ANOVA followed by Tukey's post-hoc test, *p-value* <0.05. Data are represented as mean of at least 3 independent replicates ± SD (≥ 5 hydroponically grown plants per replicate).

1225

1226

1227

1228

1229

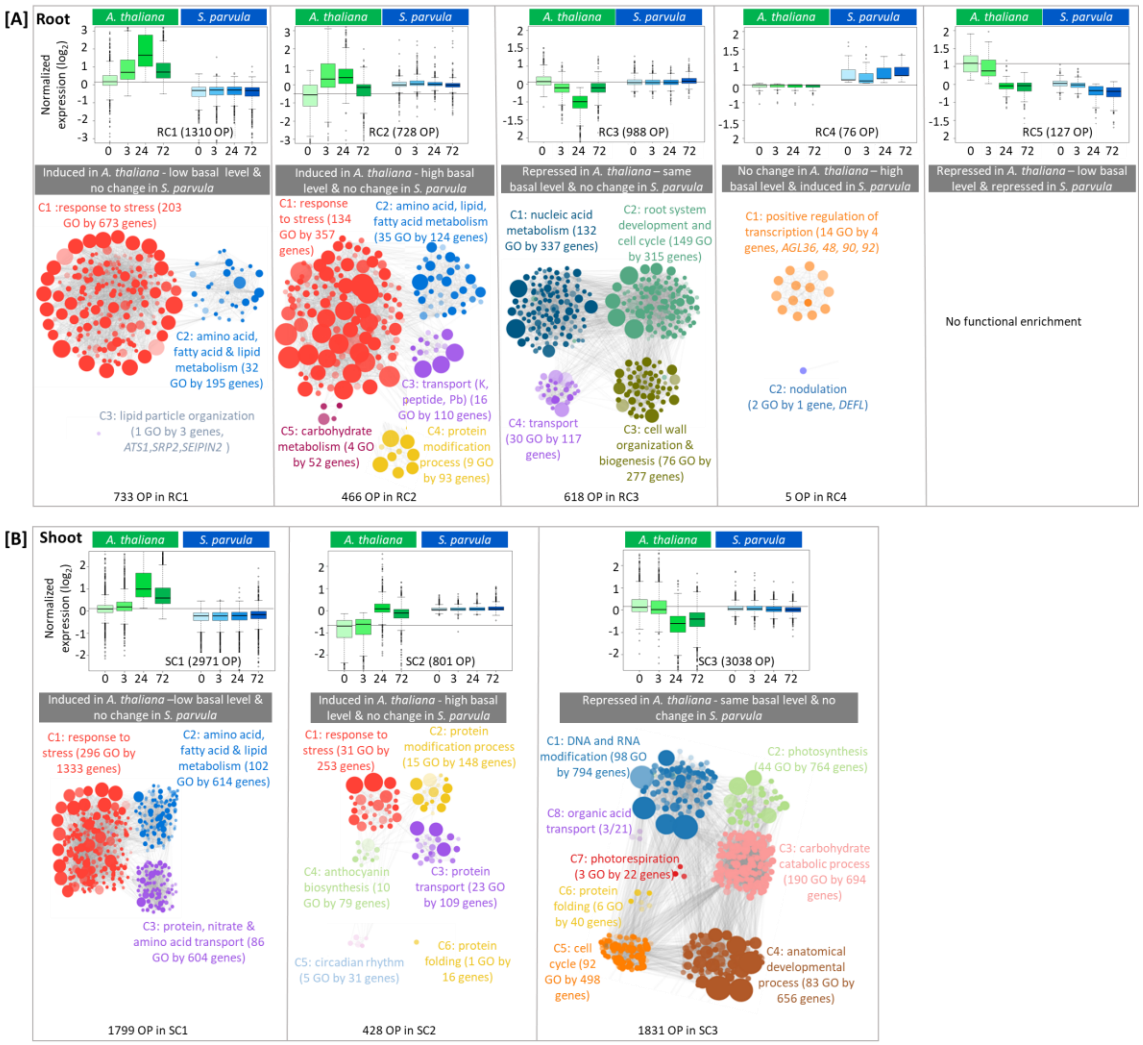

Figure 8. Co-expressed ortholog gene modules highlight stress preparedness towards high K^+ stress in *S. parvula* orthologs that are constitutively expressed compared to induction or suppression of orthologs in *A. thaliana*. Normalized gene expression clusters of ortholog pairs (OP) between *A. thaliana* and *S. parvula* in **[A]** roots and **[B]** shoots. Fuzzy K-means clustering was used to find temporally co-regulated clusters with a membership cutoff of ≥0.5. Box and whisker plots mark the median expression at each time point with the thick line within the box; interquartile range between first and third quartile are shown with the box; and interquartile range x 1.5 are marked by whiskers for lower and upper extremes. Basal level for 0 h in *A. thaliana* is marked by a grey line in all plots. Each cluster was used for a functional enrichment analysis represented by GOMCL summaries placed below co-expression plots. A node in each cluster represents a gene ontology (GO) term; size of a node represents the number of genes included in that GO term; the clusters that represent similar functions share the same color and are given a representative cluster name and the edges between nodes show the orthologs that are shared between functions. All clusters included in the network have adj p-values <0.05 with false discovery rate correction applied. More significant values are represented by darker nodes.

1230

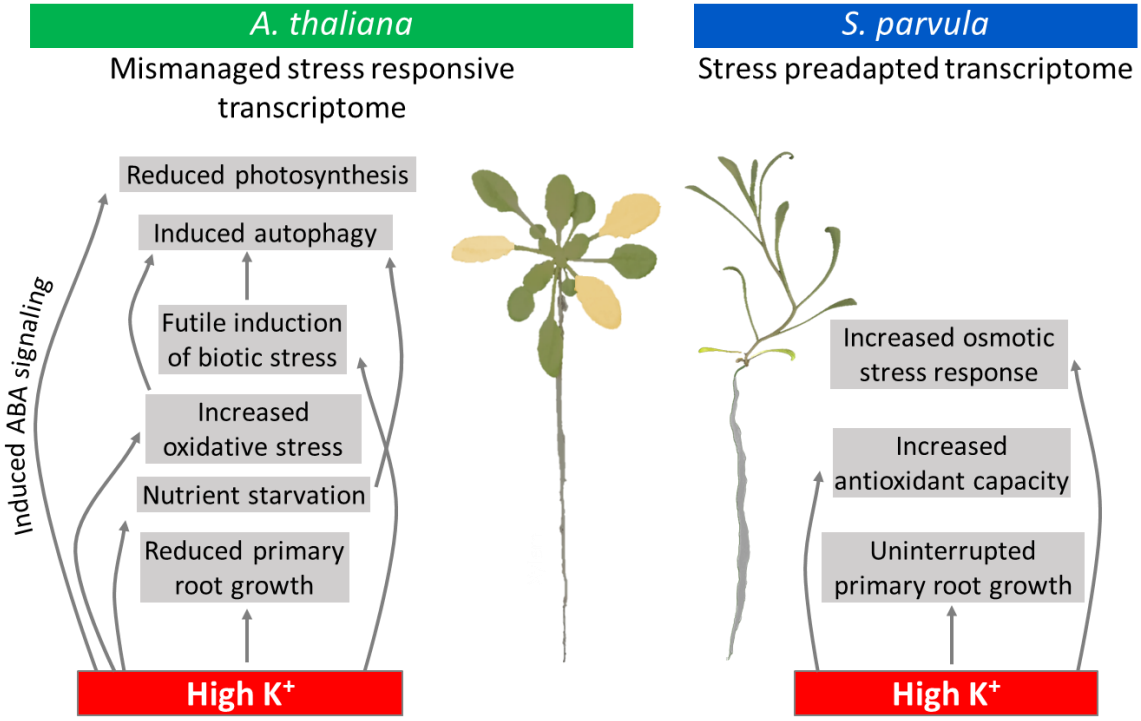

Figure 9. Deterministic cellular processes in surviving high K^+ stress.

1231
1232
1233
1234
1235
1236
1237
1238
1239
1240
1241
1242
1243
1244
1245

1246 **Supplementary figures**

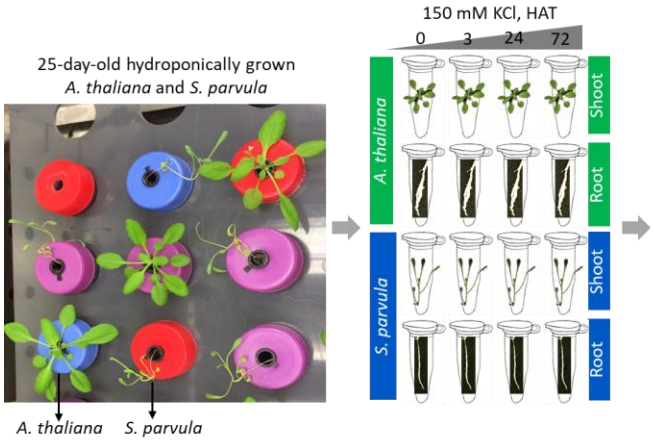

Experiment	# replicates per condition	Total number of samples
Ionome	4	64
Transcriptome	3	48
Metabolome	4	48

Figure S1. Sampling scheme for the ionome, metabolome, and transcriptome experiments performed in this study. 25-day-old *Arabidopsis thaliana* and *Schrenkiella parvula* plants were grown in 1/5th Hoagland's solution with/without 150 mM KCl for up to 72 hours after treatment (HAT). All samples were 28-day-old at the time of sample harvest. Both ionome and metabolome profiles have 4 biological replicates and transcriptome samples have 3 biological replicates. Each replicate contains tissues from at least 5 different plants.

1247

1248

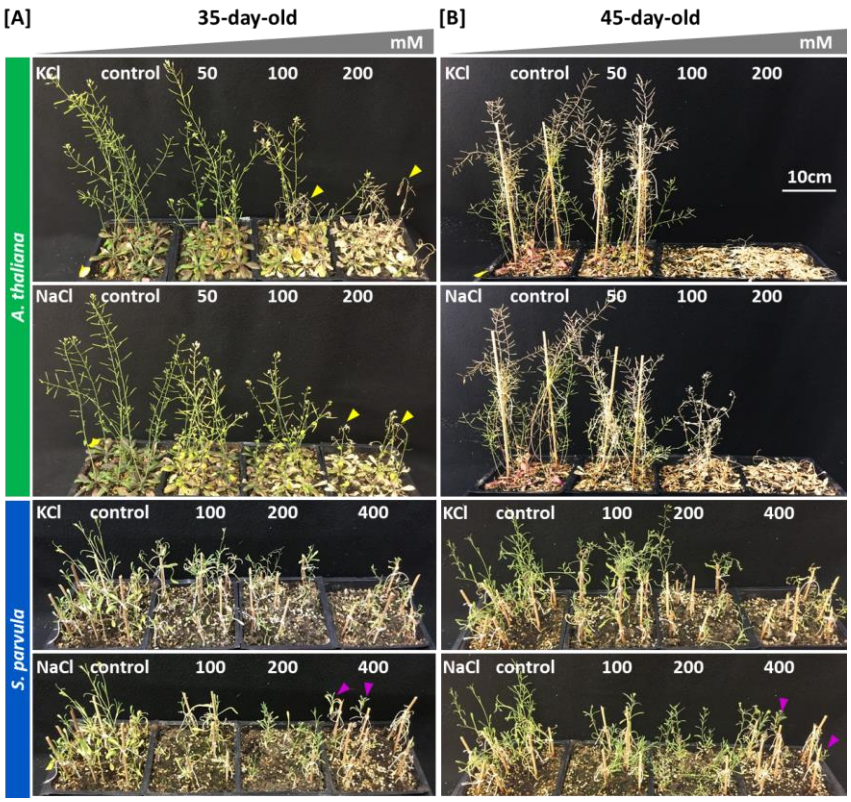

Figure S2. KCl is more toxic than NaCl at the same osmotic strength. [A] 21-day-old plants treated for 35 days every other day. Yellow arrow heads indicate visibly wilting shoots only in KCl treated plants. **[B]** The same plants imaged after 10 days show 100 mM KCl treated plants did not survive while 100 mM NaCl treated plants appear to be stressed but not dead in *A. thaliana*. In *S. parvula* 400 mM KCl treated plants did not develop any flower while 400 mM NaCl treated plants flowered and developed seeds (indicated with purple arrow heads).

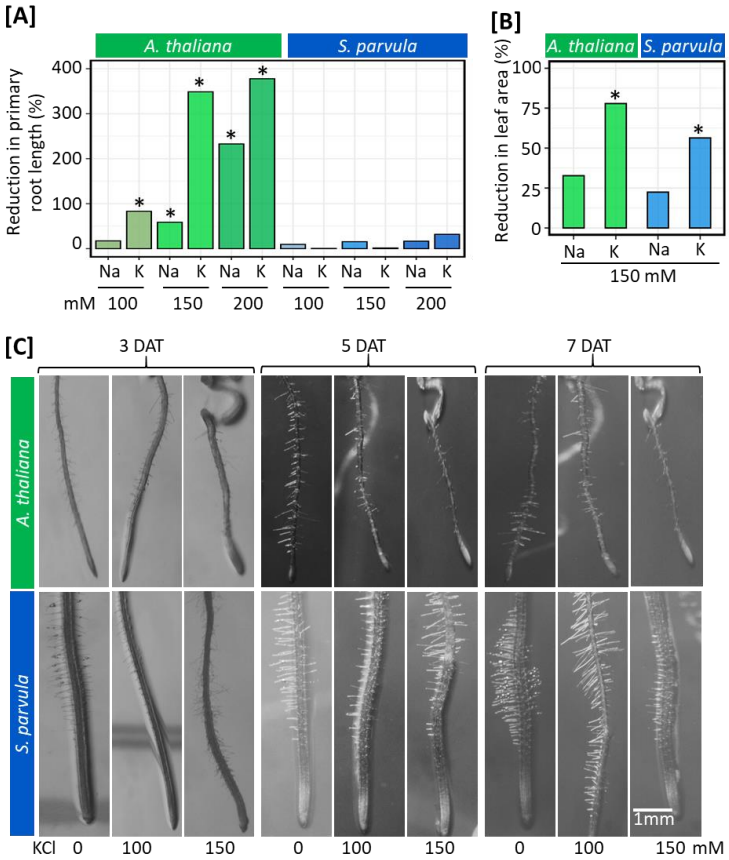

Figure S3. Reduction in primary root length **[A]** and leaf area **[B]** upon Na and K treatment. Primary root length was measured on 17-day-old seedlings grown on 1/4 MS media supplemented with 0 to 200 mM NaCl and KCl based on a 12-day treatment of NaCl or KCl. Leaf area was measured for 5- and 6-week-old hydroponically grown *A. thaliana* and *S. parvula* treated with increasing levels of NaCl and KCl for 1- and 3-weeks respectively. Minimum 5 plants per condition used in A and a minimum of 3 plants per condition used for B. **[C]** Representative images showing the effect of KCl on root hair growth in *A. thaliana* and *S. parvula*. Scale bars are 1 mm for all the panels. Seeds were germinated in 1/4th MS and transferred to the corresponding plates with 100 or 150 mM KCl 5 days after germination. Same roots were photographed on 3, 5, and 7 DAT. DAT-Days after treatment. Asterisks indicate significant changes between the treated samples to its respective control samples (t-test with $p < 0.05$). DAT-Days after treatment.

[A]

	A. thaliana					*S. parvula*				
	Enriched processes	Total # of metabolites	# of MACs*	P-value	P-adj	Enriched processes	Total # of metabolites	# of MACs*	P-value	P-adj
Root	Galactose Metabolism	38	4	0.004	0.411	Galactose Metabolism	38	7	0.0002	0.016
	Lactose Degradation	9	2	0.011	0.533	Urea Cycle	29	6	0.0003	0.016
						Aspartate Metabolism	35	5	0.006	0.199
						Glucose-Alanine Cycle	13	3	0.009	0.22
						Ammonia Recycling	32	4	0.023	0.449
						Arginine and Proline Metabolism	53	5	0.034	0.519
						Lactose Degradation	9	2	0.037	0.519
						Malate-Aspartate Shuttle	10	2	0.045	0.555
Shoot	Enriched processes	Total # of metabolites	# of MACs*	P-value	P-adj	Enriched processes	Total # of metabolites	# of MACs*	P-value	P-adj
	Galactose Metabolism	38	7	0.0003	0.025	Galactose Metabolism	38	5	0.002	0.196
	Lactose Degradation	9	3	0.003	0.154	Lactose Degradation	9	2	0.02	0.981
	Glycerolipid Metabolism	25	4	0.011	0.26	Glucose-Alanine Cycle	13	2	0.041	1
	Glycolysis	25	4	0.011	0.26					
	Lactose Synthesis	20	3	0.032	0.553					
	Gluconeogenesis	35	4	0.034	0.553					

Significantly enriched process

*Metabolites that significantly changed in abundance

[B]

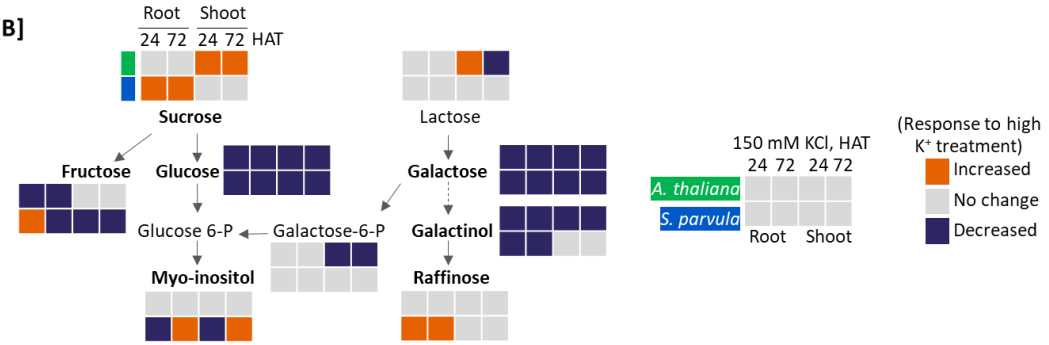

Figure S4. Carbohydrate and nitrogen metabolism related processes were enriched in *S. parvula* roots. **[A]** Enriched metabolic pathways in *A. thaliana* and *S. parvula* in response to excess K stress. Metabolite Enrichment Analysis was performed with MetaboAnalyst with a p-adj cut off set to < 0.05. p-values were adjusted using Benjamini-Hochberg correction for multiple testing. **[B]** Simplified galactose metabolism pathway. The seven metabolites that significantly changed in abundance and quantified using GC-MS are indicated in bold font.

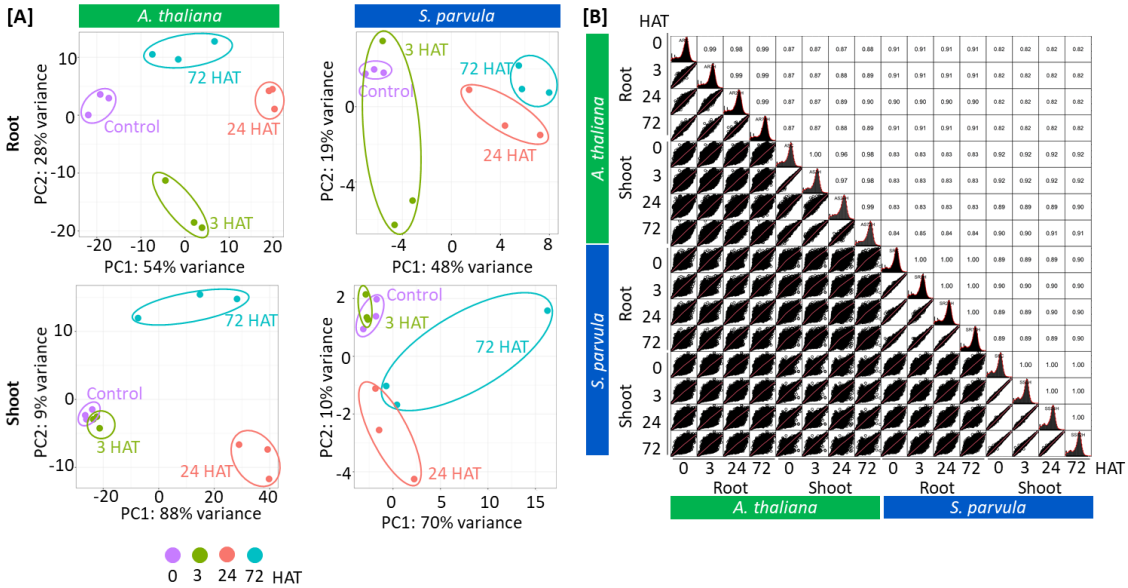

Figure S5. **Overview of transcriptomes in each condition tested in response to high K stress in *A. thaliana* and *S. parvula* roots. [A]** Principal component analysis (PCA) for 0, 3, 24, and 72 hours after treatment (HAT) for *A. thaliana* (left panel) and *S. parvula* roots and shoots. **[B]** Overall transcript level correlation between conditions. Correlation plots were generated using PerformanceAnalytics library in R 4.0.2. Pearson correlation coefficient is given within plots for each comparison.

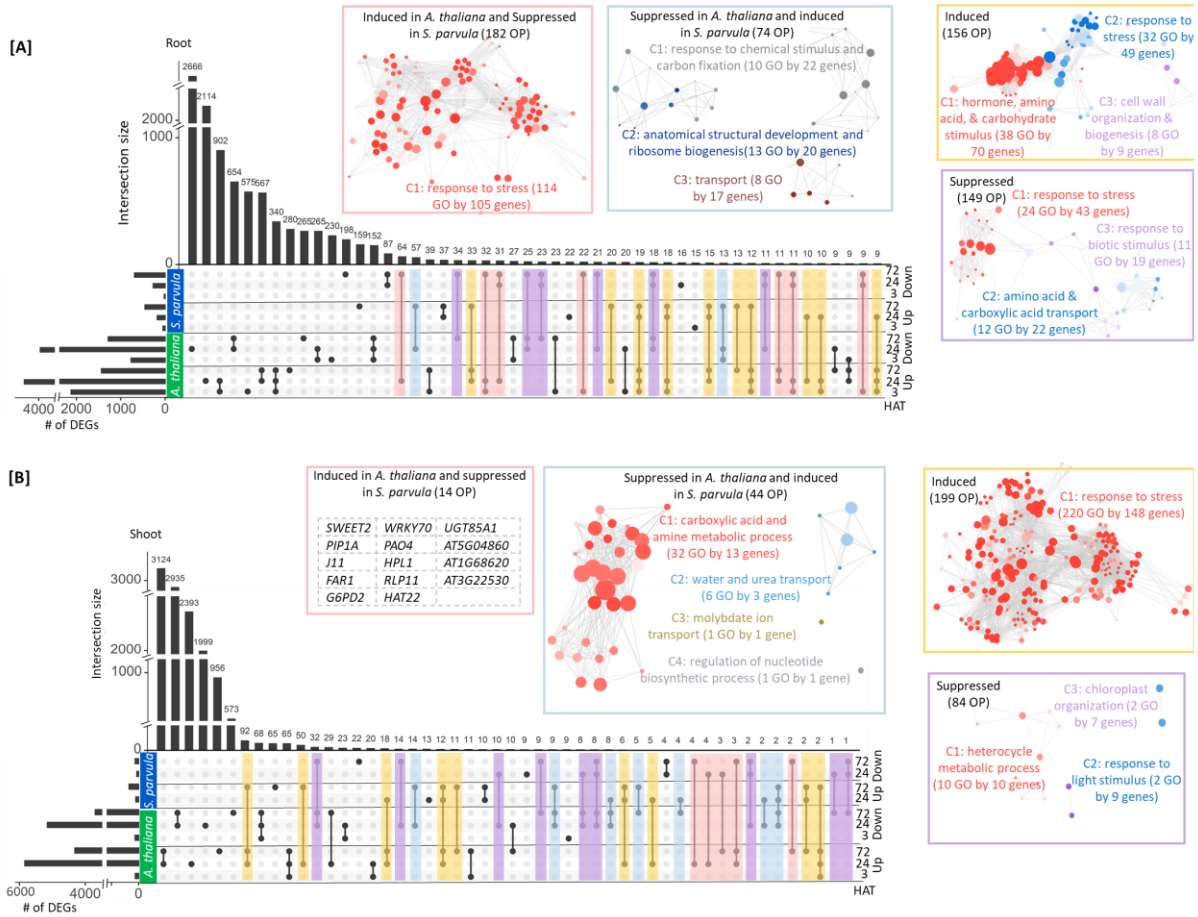

Figure S6. **The majority of differentially expressed genes (DEGs) show species specific responses followed by tissue and response time specificity.** Differentially expressed genes (DEGs) between *A. thaliana* and *S. parvula* for **[A]** roots and **[B]** shoots. Enriched functions are highlighted for diametric and shared responses between differently regulated ortholog pairs (OP). DEGs at each time point were called using DESeq2 compared to 0 h with a p-adj value based on Benjamini-Hochberg correction for multiple testing set to <0.01. The shared genes were plotted using UpsetR in R 4.0.2.

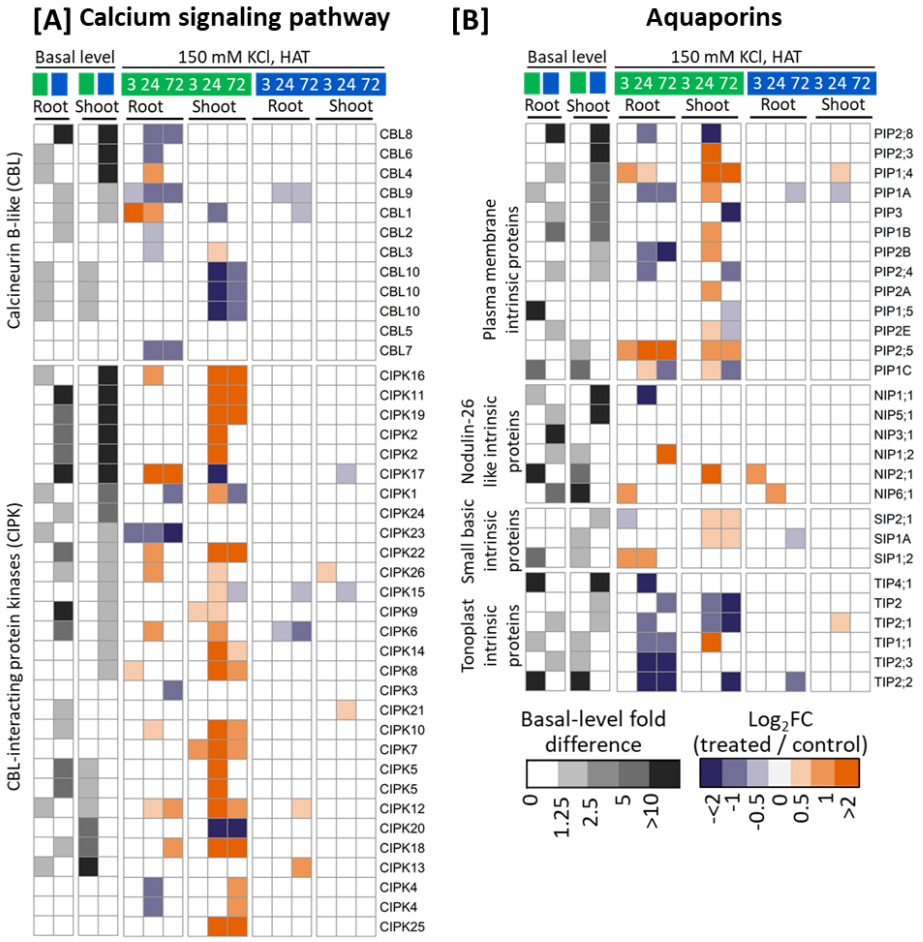

Figure S7. Genes coding for calcium signaling and aquaporins are differently regulated during high K^+ stress. Genes associated with **[A]** calcium signaling pathway and **[B]** aquaporins during high K^+ in root and shoot of *A. thaliana* and *S. parvula*. The significantly changed genes at least in one condition are presented in the heatmap. DEGs at each time point were called using DESeq2 compared to 0 h with a p-adj value based on Benjamini-Hochberg correction for multiple testing set to <0.01.

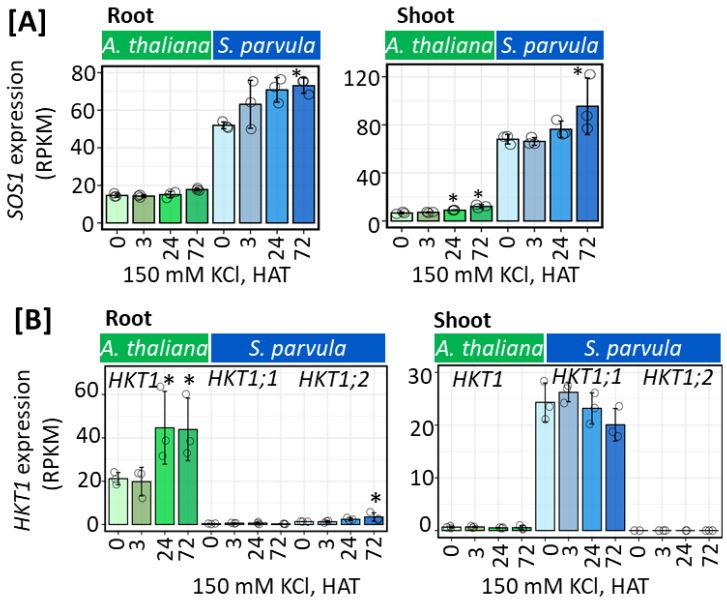

Figure S8. Normalized expression of [A] *SOS1* and [B] *HKT1* in roots and shoots of *A. thaliana* and *S. parvula* under 150 mM KCl treatments. *HKT1* has undergone a tandem duplication in *S. parvula,* and *SpHKT1;2* is known to function in selective K^+ transport. *AtHKT1* and *SpHKT1;1* are selective Na transporters. * represent DEGs at each time point called using DESeq2 compared to 0 h with a p-adj value based on Benjamini-Hochberg correction for multiple testing set to <0.01.

Supplementary tables

Table S1. Relative abundance of metabolites for *A. thaliana* and *S. parvula* roots and shoots sample. 25-days-old hydroponically grown seedlings were treated for 24 and 72 hours after 150 mM KCl treatment and control samples were harvested together with the treated samples. Data are represented as the mean of at least 3 independent replicates. ≥5 plants per replicate were used.

Table S2. Number of total reads and percentage of uniquely mapped reads to *A. thaliana* (TAIR10) or *S. parvula* v2.2 gene models for root and shoot transcriptomes under high K^+. At- *A. thaliana,* Sp- *S. parvula*, C- control, 3- 3 hours after treatment, 24- 24 hours after treatment, 72- 72 hours after treatment, R- root samples, S- shoot samples. 25-days-old hydroponically grown seedlings were treated for 3, 24, and 72 h after 150 mM KCl treatment. Control samples were harvested together with the treated samples. Data are represented as the mean of at least 3 independent replicates. ≥5 plants per replicate were used.

1280 **Table S3.** List of differentially expressed genes (DEGs) in 3, 24, and 72 hours after treatment
1281 (HAT) in *A. thaliana* and *S. parvula* root and shoot. DEGs were called using DESeq2 with a *p*-adj
1282 value based on Benjamini-Hochberg correction for multiple testing set to <0.01. Data are
1283 represented as mean of 3 independent replicates ± SD given using ≥ 5 hydroponically grown
1284 plants per replicate.
1285 **Table S4.** Enriched biological processes for a non-redundant set of induced and suppressed
1286 DEGs for *A. thaliana* roots and shoots sample under 150 mM KCl. DEGs were functionally
1287 annotated by a Gene Ontology (GO) enrichment test using BinGO in Cytoscape and enriched
1288 biological processes were further clustered based on shared genes using GOMCL with adj *p*-
1289 value <0.05 after false discovery rate correction with Benjamini-Hochberg correction.
1290 **Table S5.** Enriched biological processes for time point-specific DEGs (3, 3&24+24, 24&72, 72,
1291 and 3&24&72) for *A. thaliana* roots sample under 150 mM KCl. DEGs were functionally
1292 annotated by a Gene Ontology (GO) enrichment test using BinGO in Cytoscape and enriched
1293 biological processes were further clustered based on shared genes using GOMCL with adj *p*-
1294 value <0.05 after false discovery rate correction with Benjamini-Hochberg correction.

1295 **Table S6.** Enriched biological processes for time point-specific DEGs (3, 3&24+24, 24&72, 72,
1296 and 3&24&72) for *A. thaliana* shoots sample under 150 mM KCl. DEGs were functionally
1297 annotated by a Gene Ontology (GO) enrichment test using BinGO in Cytoscape and enriched
1298 biological processes were further clustered based on shared genes using GOMCL with adj *p*-
1299 value <0.05 after false discovery rate correction with Benjamini-Hochberg correction.

1300 **Table S7.** Enriched biological processes for time point-specific (3, 3&24, 24, 24&72, 72, and
1301 3&24&72) induced and suppressed DEGs for *A. thaliana* roots sample under 150 mM KCl. DEGs
1302 were functionally annotated by a Gene Ontology (GO) enrichment test using BinGO in
1303 Cytoscape and enriched biological processes were further clustered based on shared genes
1304 using GOMCL with adj *p*-value <0.05 after false discovery rate correction with Benjamini-
1305 Hochberg correction.

1306 **Table S8.** Enriched biological processes for time point-specific (3, 3&24, 24, 24&72, 72, and
1307 3&24&72) induced and suppressed DEGs for *A. thaliana* shoots sample under 150 mM KCl.

1308 DEGs were functionally annotated by a Gene Ontology (GO) enrichment test using BinGO in
1309 Cytoscape and enriched biological processes were further clustered based on shared genes
1310 using GOMCL with adj *p*-value <0.05 after false discovery rate correction with Benjamini-
1311 Hochberg correction.
1312 **Table S9.** Enriched biological processes for diametric responses (*i.e.* genes that are induced in
1313 one species when their orthologs are suppressed in the other species) in *A. thaliana* and *S.*
1314 *parvula* roots and shoots sample under 150 mM KCl. The pattern is extracted from Fig S6. DEGs
1315 were functionally annotated by a Gene Ontology (GO) enrichment test using BinGO in
1316 Cytoscape and enriched biological processes were further clustered based on shared genes
1317 using GOMCL with adj *p*-value <0.05 after false discovery rate correction with Benjamini-
1318 Hochberg correction.
1319 **Table S10.** Enriched biological processes for a non-redundant set of induced and suppressed
1320 DEGs for *S. parvula* roots and shoots sample under 150 mM KCl. The *S. parvula* DEG orthologs
1321 with *A. thaliana* were functionally annotated by a Gene Ontology (GO) enrichment test using
1322 BinGO in Cytoscape and enriched biological processes were further clustered based on shared
1323 genes using GOMCL with adj *p*-value <0.05 after false discovery rate correction with Benjamini-
1324 Hochberg correction.
1325 **Table S11.** Normalized gene expression clusters of ortholog pairs (OP) between *A. thaliana* and
1326 *S. parvula* in roots and shoots sample. Fuzzy K-means clustering was used to find temporally co-
1327 regulated clusters with a membership cutoff of >0.5. From initially identified 10 root and 11
1328 shoot clusters, we filtered out clusters that did not show a response to K treatments in both
1329 species and identified 5 root (RC1, RC2, RC3, RC4, and RC5) and 3 shoot (SC1, SC2, and SC3) co-
1330 expression superclusters with distinct response trends. The orthologs from each cluster were
1331 functionally annotated by a Gene Ontology (GO) enrichment test using BinGO in Cytoscape and
1332 enriched biological processes were further clustered based on shared genes using GOMCL with
1333 adj *p*-value <0.05 after false discovery rate correction with Benjamini-Hochberg correction.